

**DEVELOPMENT OF A
WEARABLE SELF-POWERED SENSOR
USING TRIBOELECTRIC MECHANISM FOR
HUMAN-MACHINE INTERACTION**

JOEY YEO JOO SII

UNIVERSITI TUNKU ABDUL RAHMAN

**DEVELOPMENT OF A WEARABLE SELF-POWERED SENSOR
USING TRIBOELECTRIC MECHANISM FOR
HUMAN-MACHINE INTERACTION**

JOEY YEO JOO SII


**A project report submitted in partial fulfilment of the
requirements for the award of Bachelor of Mechatronics
Engineering with Honours**

**Lee Kong Chian Faculty of Engineering and Science
Universiti Tunku Abdul Rahman**

May 2023

DECLARATION

I hereby declare that this project report is based on my original work except for citations and quotations which have been duly acknowledged. I also declare that it has not been previously and concurrently submitted for any other degree or award at UTAR or other institutions.

Signature : 

Name : JOEY YEO JOO SII


ID No. : 1804209

Date : 20 May 2023

APPROVAL FOR SUBMISSION

I certify that this project report entitled **“DEVELOPMENT OF A WEARABLE SELF-POWERED SENSOR USING TRIBOELECTRIC MECHANISM FOR HUMAN-MACHINE INTERACTION”** was prepared by **JOEY YEO JOO SII** has met the required standard for submission in partial fulfilment of the requirements for the award of Bachelor of Mechatronics Engineering with Honours at Universiti Tunku Abdul Rahman.

Approved by,

Signature : 

Supervisor : Dr Low Jen Hahn
Date : 20/5/2023

The copyright of this report belongs to the author under the terms of the copyright Act 1987 as qualified by Intellectual Property Policy of Universiti Tunku Abdul Rahman. Due acknowledgement shall always be made of the use of any material contained in, or derived from, this report.

© 2023, JOEY YEO JOO SII. All right reserved.

ACKNOWLEDGEMENTS

I would like to thank everyone who had contributed to the successful completion of this project. I would like to express my gratitude to my research supervisor, Dr. Low Jen Hahn for his invaluable advice, guidance and his enormous patience throughout the development of the research.

In addition, I would also like to express my gratitude to my loving parents and friends who had helped and given me encouragement to complete my final year project when I faced many obstacles.

ABSTRACT

Rapid development of internet of things (IoT) has induced high demand for human-machine interaction (HMI) devices. Sensors as the device to detect physical parameters and convert them into electrical signal act an important role in HMI applications. Wearable devices is one of the famous HMI applications on-trend. Conventional sensors that are rigid, inflexible, and required bulky power sources become incompatible with wearable devices especially when it comes to seamless contact with soft and irregular surfaces such as human skin. Therefore, triboelectric nanogenerators (TENG) with stretchable materials are introduced. Through a triboelectric mechanism, TENG can transform mechanical energy into electrical energy. The generated potential difference can be used as a signal, making TENG a sensor that works independently and does not rely on a power supply. Ecoflex, a type of silicone rubber, is proposed as the contact material with skin for the wearable self-powered sensor. The sensor operates by contact separation between the two materials and by single electrode mode. A simulation has been done, proving possibilities of using Ecoflex as contact materials and copper as electrode. The fabricated sensor can generate potential differences in the range of approximately -500 mV to 700 mV. The sensor can generate voltage based on the force applied on the sensor through tapping. The sensor is applied in human-machine interface (HMI) applications, which are to control the height of ball bouncing based on the voltage generated and control which light-emitting diodes (LEDs) to be light up based on the frequency of the voltage in a period. The sensor has proven possibilities of TENG as a wearable self-powered sensor that can be applied in various applications.

TABLE OF CONTENTS

DECLARATION		i
APPROVAL FOR SUBMISSION		ii
ACKNOWLEDGEMENTS		iv
ABSTRACT		v
TABLE OF CONTENTS		vi
LIST OF TABLES		ix
LIST OF FIGURES		x
LIST OF SYMBOLS / ABBREVIATIONS		xiii
LIST OF APPENDICES		xv
CHAPTER		
1	INTRODUCTION	1
1.1	General Introduction	1
1.2	Importance of the Study	2
1.3	Problem Statement	3
1.4	Aim and Objectives	3
1.5	Scope and Limitation of the Study	3
1.6	Contribution of the Study	4
1.7	Outline of the Report	5
2	LITERATURE REVIEW	6
2.1	Introduction	6
2.2	Introduction to Self-powered Mechanism	6
2.2.1	Photovoltaic	6
2.2.2	Electromagnetic Generator	7
2.2.3	Biofuel Cells	8
2.2.4	Radio-frequency	9
2.2.5	Thermoelectric Generator	9
2.2.6	Piezoelectric Nanogenerator	10
2.3	Introduction to Triboelectric Nanogenerators	11

2.4	Working Modes of Triboelectric Nanogenerators	12
2.4.1	Vertical Contact Separation Mode	12
2.4.2	Sliding Mode	13
2.4.3	Single Electrode Mode	14
2.4.4	Free Standing Mode	15
2.5	Factors Affecting Performance of Triboelectric Nanogenerators	17
2.5.1	Choice of Materials	17
2.5.2	Surface Area of Contact	18
2.5.3	Humidity	20
2.5.4	Temperature	21
2.6	Flexible Triboelectric Nanogenerators as Wearable Sensor for Human-machine Interaction	21
2.6.1	Polydimethylsiloxane (PDMS)	21
2.6.2	Ecoflex	23
2.7	Summary	24
3	METHODOLOGY AND WORK PLAN	25
3.1	Introduction	25
3.2	Simulation of Self-powered Sensor	25
3.2.1	Contact Separation Mode	25
3.2.2	Single Electrode Mode	26
3.3	Fabrication of Self-powered Sensor	27
3.3.1	Materials	27
3.3.2	Conceptual Design	28
3.3.3	Fabrication Process	28
3.4	Characterization of the Self-powered Sensor	30
3.5	Human-machine Interaction Applications of the Self-powered Sensor	32
3.5.1	Ball Bouncing Application	32
3.5.2	Turn On LED Application	34
3.6	Summary	35
4	RESULTS AND DISCUSSION	36
4.1	Introduction	36
4.2	Simulation	36

4.3	Characterization	40
4.4	Human-machine Interaction Applications	43
4.5	Summary	45
5	CONCLUSIONS AND RECOMMENDATIONS	46
5.1	Conclusions	46
5.2	Recommendations for Future Work	46
	REFERENCES	48
	APPENDICES	52

LIST OF TABLES

Table D-1:	Potential Difference (V) Generated by Contact Separation Mode of TENG. (Triboelectric Material: PDMS, Electrode: Copper)	59
Table D-2:	Potential Difference (V) Generated by Contact Separation Mode of TENG. (Triboelectric Material: EGaIn Ecoflex, Electrode: Copper)	60
Table D-3:	Potential Difference (V) Generated by Contact Separation Mode of TENG. (Triboelectric Material: PDMS, Electrode: Silver)	61
Table D-4:	Potential Difference (V) Generated by Contact Separation Mode of TENG with Different Triboelectric Materials and Electrodes.	62
Table D-5:	Potential Difference (V) Generated by Single Electrode Mode of TENG with Different Triboelectric Materials and Electrodes.	63
Table D-6:	Potential Difference (V) Generated by Single Electrode Mode of TENG for Distance up to 58 mm.	64

LIST OF FIGURES

Figure 2.1:	Schematic Illustration of Photovoltaic Textile (Zhang et al., 2016).	7
Figure 2.2:	A Electromagnetic Generator for Harvesting Energy from Human Motion (Saha et al., 2008).	8
Figure 2.3:	Schematic Drawing of Enzymatic Biofuel Cells (Xiao, 2022).	9
Figure 2.4:	(a) Working Mechanism of Thermoelectric Generators (Jia et al., 2021). (b) Schematic Diagram of Flexible Thermoelectric Generator.	10
Figure 2.5:	Equivalent Circuit Model of TENG (Wu et al., 2019).	11
Figure 2.6:	Contact Separation Mode TENG Mechanism (Fan et al., 2012).	13
Figure 2.7:	Sliding Mode TENG Mechanism (Lin et al., 2016).	14
Figure 2.8:	Single Electrode Mode TENG Mechanism (Khan et al., 2019).	15
Figure 2.9:	Mechanism of Free Standing Mode TENG (Lin et al., 2016).	16
Figure 2.10:	Free Standing Mode TENG with (a) Dielectric-conductor Configuration in Non-contact Sliding Mode. (b) Dielectric-dielectric Configuration (Lin et al., 2016).	16
Figure 2.11:	Statistics on Materials used in Fabricating TENG from 100 Articles. (A) Fraction of Electron Acceptors. (B) Fraction of Electron Donors (Zhang and Olin, 2020).	18
Figure 2.12:	Simulation of TENG with Dome and Pillar Array Structure (Tcho et al., 2017).	19
Figure 2.13:	Sponge-based TENG (Goh et al., 2021)	19
Figure 2.14:	Optical Micrographs of TENG: (a) LD-MN, (b) HD-MN, and (c) OL-MN (Chung and Ke, 2020).	20
Figure 2.15:	Schematic of Finger Motion Sensor by Dhakar et al. (2016).	22
Figure 2.16:	Self-powered Tactile Sensor in Matrix Form by(Yang et al., 2013).	22

Figure 2.17:	Orbicularis Oculi's Sensor Design and Placement. (Anaya et al., 2020)	24
Figure 3.1:	Schematic Diagram of Simulation Model for Contact Separation Mode.	26
Figure 3.2:	Schematic Diagram of Simulation Model for Single Electrode Mode.	27
Figure 3.3:	Conceptual Design of the Self-powered Sensor.	28
Figure 3.4:	Molds created using Solidworks and 3D printed.	28
Figure 3.5:	Ecoflex 00-50 Solution.	29
Figure 3.6:	Molding Process of the Self-powered Sensor.	29
Figure 3.7:	Self-powered Sensor Fabricated.	29
Figure 3.8:	National Instrument (NI) ELVIS II+ Board.	30
Figure 3.9:	Voltage Divider Circuit used in Data Collection.	31
Figure 3.10:	Block Diagram Built in LabVIEW.	31
Figure 3.11:	Circuit Diagram for Ball Bouncing Application.	33
Figure 3.12:	Circuit Diagram for Turn on LED Application.	35
Figure 4.1:	Electric Potential Distribution for Simulation of TENG in Contact Separation Mode when Distance (D) between the Contact Surface of Elastomer and Skin Increases.	37
Figure 4.2:	Graph of Distance against Potential Difference for Simulation of TENG in Contact Separation Mode.	37
Figure 4.3:	Electric Potential Distribution for Simulation of TENG in Single Electrode Mode when Distance (D) between the Contact Surface of Elastomer and Skin Increases.	38
Figure 4.4:	Graph of Distance against Potential Difference for Simulation of TENG in Single Electrode Mode.	39
Figure 4.5:	Graph of Distance against Potential Difference for Simulation of TENG in Single Electrode Mode for Distance up to 60 mm.	40
Figure 4.6:	Sensor Output during Pressing and Releasing.	41
Figure 4.7:	Working Mechanism of Self-powered Sensor.	41

Figure 4.8:	Signal Output when Continuous Tapping from Hand on Sensor.	42
Figure 4.9:	Signal Output when Tapped with Different Force on Sensor.	42
Figure 4.10:	Signal Output when Tapped with Different Frequency on Sensor within a Specified Time Frame.	43
Figure 4.11:	Outcome of Ball Bouncing Application.	44
Figure 4.12:	Outcome of Turn On LED Application.	44
Figure B-1:	Triboelectric Series of Polymers, Metals, and Inorganic Compounds (Gooding and Kaufman, 2011).	52
Figure C-1:	Flowchart for Ball Bouncing Application.	53
Figure D-1:	Flowchart for Turn On LED Application.	56

LIST OF SYMBOLS / ABBREVIATIONS

v	final velocity, m/s
u	initial velocity, m/s
a	acceleration, m/s ²
s	distance, m
t	time, s
IoT	Internet of things
HMI	Human-machine interaction
TENG	Triboelectric nanogenerator
EMG	Electromagnetic generator
NdFeB	Neodymium magnets
BC	Biofuel cells
RF	Radio-frequency
TEG	Thermoelectric generator
DC	Direct current
PENG	Piezoelectric nanogenerator
PDMS	Polydimethylsiloxane
PVDF	Polyvinylidene fluoride
PET	Polyethylene terephthalate
AC	Alternating current
FEP	Fluorinated ethylene propylene
PTFE	Polytetrafluoroethylene
Al	Aluminium
Cu	Copper
EGaIn	Eutectic gallium indium
LD-MN	Low density microneedle
HD-MN	High density microneedle
OL-MN	Overlapped microneedle
DT-HMI	Delta-parallel-inspired human-machine interface
VR	Virtual reality
AR	Augmented reality
PEDOT:PSS	Poly(3,4-ethylenedioxythiophene) polystyrene sulfonate

ITO	Indium tin oxide
PLA	Polylactic Acid
STL	Stereolithography
DMM	Digital Multimeter

LIST OF APPENDICES

Appendix A: Supporting Attachment for Literature Review	52
Appendix B: Supporting Attachments for Ball Bouncing Application	53
Appendix C: Supporting Attachments for Turn On LED Application	56
Appendix D: Tables of Simulation Results	59

CHAPTER 1

INTRODUCTION

1.1 General Introduction

Internet of things (IoT) has gained increasing attention in recent years. This has also induced one of the popular discussions relating to wearable devices. Wearable devices will acquire physical parameters from human motion for applications such as human motion recognition, human-machine interaction (HMI), and energy harvester. As a product that comes into direct contact with humans, comfort, and safety are top priorities. Consequently, sensors serve important roles to obtain the physical parameters from the user.

From that, triboelectric nanogenerators (TENG) have gained prominence as one of the useful energy harvesting technologies that can be applied to wearable technologies as self-powered sensors. The idea of TENG was first proposed by Fan et al. (2012). The concept behind this technology is to convert mechanical energy from everyday life to electrical energy by triboelectric mechanism. An example of a triboelectric mechanism that will commonly see in life is hair lifting after combing. This is due to contact electrification, which occurs when the hair is charged after separating from the comb with which it was previously in contact. With this concept, Fan et al. (2012) proposed using two materials with distinct different triboelectric characteristics, while using metal as electrode attached on the materials. As a result, a triboelectric potential layer formed, causing electrons to flow in an external load. The TENG has output voltage and demonstrated its ability to harvest energy from various dynamic motions. Following that, many researchers became interested in further development of TENG in various applications.

Following the trends, TENG has been applied in a lot of wearable devices for human-machine interaction. However, most TENGs are fabricated with solid materials which cannot comply with the soft and irregular surface of human skin. As researchers pay attention to comfort and safety while requiring the sensor to have seamless contact with human skin for better electrification between skin and triboelectric material, flexible TENG with stretchable

materials has been proposed (Pan et al., 2020). One of the materials often used in wearable sensors is Ecoflex. It is platinum-catalyzed silicone rubber that has very strong, adhesive, and stretchable characteristics. Most importantly, it is a biocompatible material that can mount on human skin without causing discomfort or skin irritation (Amjadi et al., 2015).

In this project, a wearable self-powered sensor is developed using a triboelectric mechanism. A sandwich structure flexible TENG with Ecoflex as triboelectric materials and copper as electrode is fabricated. The sensor operates by contact separation between human skin and the Ecoflex surface or through tapping with a hand. The sensor works in single electrode mode TENG. During tapping, the Ecoflex will become negatively charged and the copper electrode become positively charged. Thus, the copper electrode will tend to send electrons out so that the Ecoflex and copper will be in the equilibrium state, resulting in an output voltage over the external load. The voltage generated will be treated as a signal and collected to be applied in HMI applications.

1.2 Importance of the Study

The self-powered sensor is essential as it is helpful in the renewable energy field and energy harvesting technologies. With further study on this topic, more devices can implement the use of self-powered sensors to be the main power sources of the devices. If all the components of the devices can be driven by the power generated by TENG, that means the devices do not need any external power sources or charging for continuous usage of the device. In the long term, this is reducing the environmental and human health issue due to power generated from fossil fuels.

TENG with flexible material is currently famous in several applications such as health monitoring devices, wearable electronics, and soft robotics. This is due to the flexible properties making it durable in most applications while providing a better life cycle for the devices.

The study of sensors can be useful in a lot of human-machine interface applications and osteoarthritis habitation applications. The development of this approach will benefit a lot of applications due to its properties of flexibility and independent from power sources.

1.3 Problem Statement

Conventional sensors are rigid and inflexible. Conventional sensors' materials are mostly metal, semiconductor, or carbon which are rigid but brittle at the same time. These materials are least sustainable and will be easily damaged by external forces exceeding the strain limits on the sensors. Therefore, conventional sensors cannot be used in flexible sensing devices. The stretchable feature can reduce this issue while not affecting its performance. The flexible and stretchable sensors can perform tasks similar to human tissues, therefore they can be used in human motion detection (Nguyen et al., 2021).

Furthermore, conventional sensors required power sources to operate. Portable power sources such as batteries are bulky which has limited the flexibility of designing a product. In the meantime, these power sources are mainly generated by the combustion of fossil fuels to produce this non-renewable energy. Thus, it is increasing environmental degradation and threatening human health. Additionally, batteries need to be charged from time to time, where it does not have a long life cycle (Wang et al., 2021c).

1.4 Aim and Objectives

The aim of this project is to develop a wearable self-powered sensor using triboelectric generated by contact-separation motion between a material with human skin. To achieve this aim, these objectives have been established:

- (i) To simulate a wearable self-powered sensor using a triboelectric mechanism.
- (ii) To characterize the self-powered sensor.
- (iii) To apply the self-powered sensor for the human-machine interaction application.

1.5 Scope and Limitation of the Study

The project covered only the development of a wearable self-powered sensor using the triboelectric mechanism for human-machine interaction. The study of TENG in contact separation mode and single electrode mode will be done through simulation through COMSOL Multiphysics. The effect of the material chosen was also investigated through the simulation. Other modes of TENG were not simulated because a wearable sensor is expected to be developed,

whereby one of the contact materials will be human skin. Therefore, the free-standing mode is not considered. Furthermore, the contact separation mode and single electrode are the simplest modes to be fabricated.

The study will only look at flexible TENG as a sensor. Although it can be used as an energy harvesting tool and to power other small-scale electronics due to its self-powered mechanism, this project will only treat the potential difference generated as a signal for the HMI applications.

To keep the design simple, only two triboelectric materials will be used on each side of the terminal in the TENG fabricated, where one of which is likely to be human skin. Thus, the power generated by the TENG fabricated is expected to be lower than those completed by other researchers due to the low possibility to give a consistent output when tapping on the sensor with a hand.

Furthermore, the sensor fabricated does not consist of a wireless function to send information out, therefore it will still require wiring to the microcontroller to check the potential difference generated by the sensor. The self-powered sensor will not be able to supply power for the microcontroller as the energy harvesting feature is not considered, therefore a power source is still needed from the microcontroller.

1.6 Contribution of the Study

This section describes the contribution of this project. The major outcomes of the projects can be summarized as follows:

Numerical simulation has been done to prove the behavior of triboelectric nanogenerators in two different working modes. The simulation has proven that contact separation mode is able to generate more voltage than single electrode mode TENG.

A wearable self-powered sensor has been fabricated using Ecoflex as the contact material and copper as an electrode. Ecoflex is a type of silicone rubber with very soft, strong, adhesive, and stretchable characteristics that can fulfill the requirement of having seamless contact with the skin. Through characterization, the sensor has proven that charged produced during contact separation of Ecoflex and skin can generate potential differences that can be

used as signals. The sensor is able to generate a voltage based on the force applied and accurately detect the frequency of tapping on it.

Two applications are designed based on the characteristics of the sensor fabricated. This has proven the possible usage of the sensor in different applications.

1.7 Outline of the Report

This report is organized into five chapters. The contents of each chapter will be covered in the following paragraph.

Chapter 1 discusses how the trend induces the development of TENG as self-powered sensors with the importance of the study of this technology. The trend of IoT has induced the use of sensors that can work independently. This chapter talks about the problem found on conventional sensors and proposed the use of flexible materials on TENG as a wearable self-powered sensor.

A review of self-powered mechanisms has been done to compare the pros and cons of each technology is given in Chapter 2. Furthermore, the basic theory behind TENG, factors affecting its performance, and wearable sensors completed by other researchers are reviewed.

Chapter 3 talks about the methodology and work plan of the project which covers four parts: simulation, fabrication, characterization, and application design. The software, materials, and equipment used are discussed in this chapter.

The results from simulation, characterization, and human-machine interaction applications are analyzed and discussed in Chapter 4. The characteristics and theory behind the self-powered sensor are explained.

Chapter 5 concludes the study of this project and proposes recommendations for possible future work.

CHAPTER 2

LITERATURE REVIEW

2.1 Introduction

This chapter first discussed a literature review of several self-powered mechanisms. Following that, working theory and different modes of triboelectric nanogenerators (TENG) are introduced. The factors affecting the performance of TENG are studied and analyzed. Some human-machine interaction applications were reviewed.

2.2 Introduction to Self-powered Mechanism

Currently, several energy harvesting techniques have been developed and widely used in human-machine interaction applications as self-powered sensors in detecting temperature, pressure, strain, and other variables. Some examples of the self-powered mechanism include photovoltaic (using solar energy), electromagnetic generators, biofuel cells, radio-frequency, thermoelectric generators, piezoelectric nanogenerators, and triboelectric nanogenerators (Sojan and Kulkarni, 2016).

2.2.1 Photovoltaic

Solar energy, as one of the commonly known clean energy sources, has been used in a lot of applications such as solar energy production, photochemical reactions, photovoltaic self-powered applications, and more. Photovoltaic self-powered can be used on wearable devices, transportation, household, and environmental monitoring equipment. This device normally consists of three parts which are the energy harvesting module (photovoltaic panel to receive solar radiation), energy conversion module, and energy storage module (Hao et al., 2022).

To apply the solid photovoltaic in wearable electronics, Zhang et al. (2016) proposed a textile structure as shown in Figure 2.1 using wire-type photoanodes and counter electrodes. The two materials are woven in interlaced structures to fulfill the wearable manner.

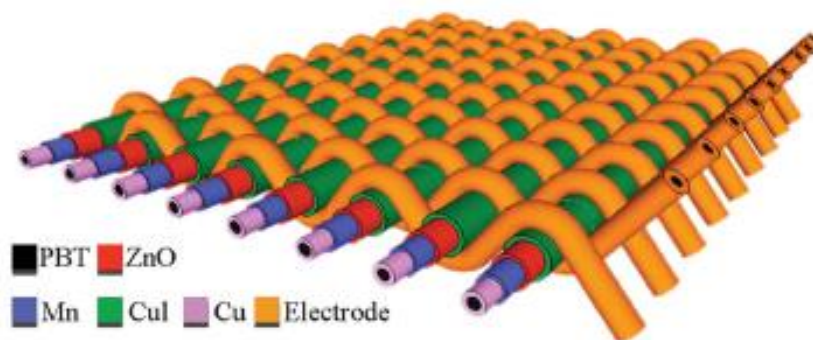


Figure 2.1: Schematic Illustration of Photovoltaic Textile (Zhang et al., 2016).

The photovoltaic self-powered are having some limitations such as the availability to track maximum power under partial shading. Some photovoltaic self-powered applications are small, thus limiting the photovoltaic panel size causing the power required by the device to be higher than the power gained. There is research done about hybrid photovoltaic mechanical energy systems to overcome the limitation mentioned. The system used TENG to harvest mechanical energy from body motion and photovoltaic to collect solar energy. Stretchable supercapacitors are used to store the energy harvested. With the hybridization of TENG and photovoltaic panels, generated electric is sufficient to operate the device (Song et al., 2019).

2.2.2 Electromagnetic Generator

The main components of the electromagnetic generator (EMG) are a series of insulated coils of wire (stator) and an electromagnetic shaft, often a magnet (rotor). Figure 2.2 shows an example of electromagnetic generator works by means of vibration by Saha et al. (2008). The device works by means of electromagnetic induction where voltage is induced in the coil while the rotor moves back and forth axially to the stator. However, EMGs are mostly rigid and bulky due to the limitation of materials used. The type of magnet used will also affect the power output. Some researchers attempted to apply EMG in wearable devices. Padasdao and Boric-Lubecke (2011) made a respiratory rate detection device by modifying a servo motor. The device is attached to the human chest, where the chest will direct contact with the armature. While the chest expands or releases, the motion turns the armature,

which will turn the gears and rotor of the motor. Thus, the current is induced. Duffy and Carroll (2004) integrated an EMG in shoe soles. Voltage is generated when Neodymium magnets (NdFeB) slide along the copper wire coil wound along the length of the shoe.

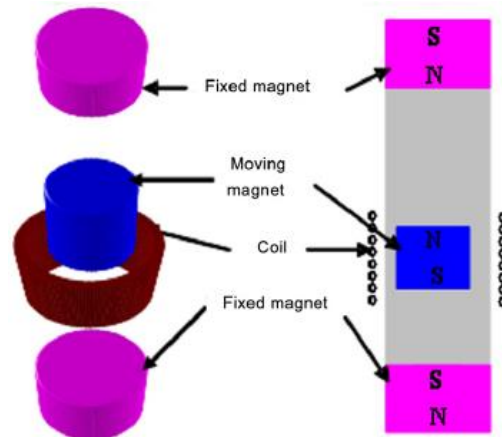


Figure 2.2: A Electromagnetic Generator for Harvesting Energy from Human Motion (Saha et al., 2008).

2.2.3 Biofuel Cells

There are two kinds of biofuel cells (BC). Microbial fuel cell drives current using bacteria and is mainly used in waste-water treatment. Enzymatic BC is a modified microbial fuel cell for wearable applications. Enzymatic BC uses enzymes as the catalyst to regulate fuel oxidation at the anode and dioxygen reduction at the biocathode as shown in Figure 2.3. Thus, chemical energy is converted into electrical energy (Xiao, 2022). The BCs as wearable devices can be used in two methods which are invasive and non-invasive. Invasive BC implant the device on human skin with a microneedle structure and are used in glucose sensing. Non-invasive BCs utilize metabolites outside of the skin such as saliva, tears, and sweat, for energy harvesting (Bandodkar and Wang, 2016). However, BCs is found to be low efficiency due to limited electron transfer (Wang et al., 2021a).

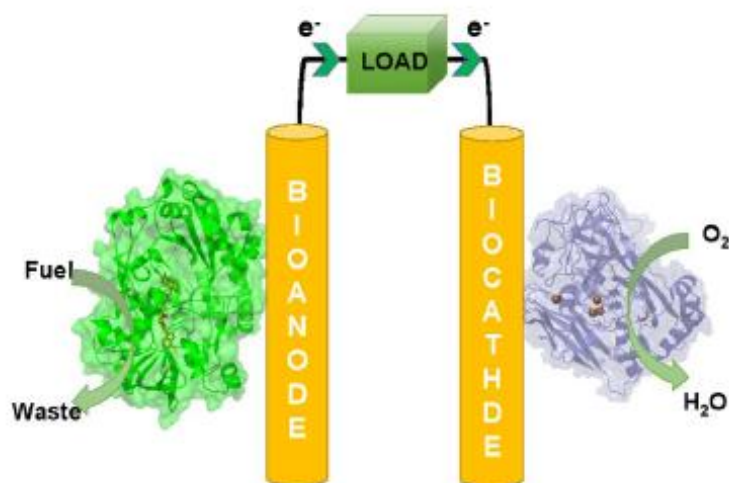


Figure 2.3: Schematic Drawing of Enzymatic Biofuel Cells (Xiao, 2022).

2.2.4 Radio-frequency

Radio-frequency (RF) antenna is a device enabling wireless transmission of signal and energy. While current trend of radio-frequency antenna is on the stretchable materials such as liquid metal or having different geometry with conventional metal. The biggest limitation of this device is the small bandwidth. When the antenna is connected to a rectifying circuit, direct current power can be generated to power sensors. However, the performance of the rectifying antenna (rectenna) become very worse during bending or stretching as the frequency is detuned at that motion (Zhu et al., 2021).

2.2.5 Thermoelectric Generator

Thermoelectric generator (TEG) is also one the energy harvester that can convert the energy from human body. However, different from PENG and TENG, TEG can produce direct current (DC) power indefinitely without the use of complex power management while it is still maintenance-free. TEG as a wearable device would convert body heat (heat energy) to electrical energy. The device would normally consist of two type of materials: p-type and n-type. As explained by Jia et al. (2021), p-type and n-type materials would diffuse from the hot surface to the cold surface. Then, they would gather at the cold surface producing thermoelectric voltage by the Seeback effect as shown in Figure 2.4 (a). One of the drawbacks of TEG is that the materials used are only solid materials. To implement this solid device on wearable electronics,

Dargusch et al. (2020) suggested attaching the TEG in small scale on flexible materials. Figure 2.4 (b) shows the schematic diagram of the proposed flexible TEG.

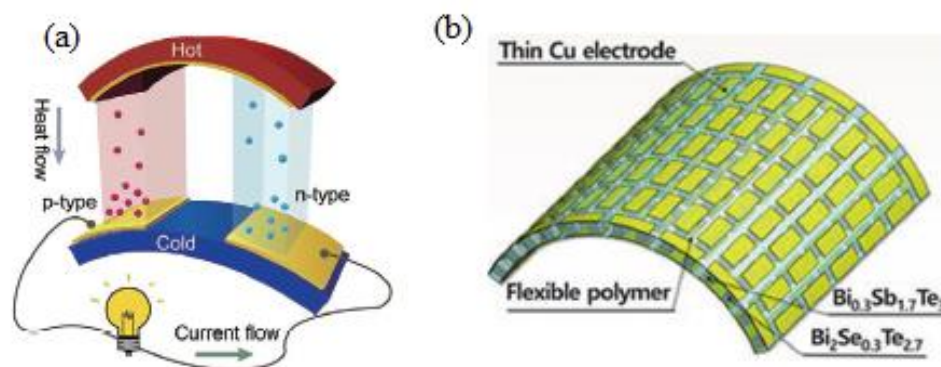


Figure 2.4: (a) Working Mechanism of Thermoelectric Generators (Jia et al., 2021). (b) Schematic Diagram of Flexible Thermoelectric Generator.

2.2.6 Piezoelectric Nanogenerator

Different from the energy harvesting tools mentioned previously, the piezoelectric nanogenerator (PENG) is able to convert mechanical energy to electrical energy in nano scale. The performance of PENG relies on the materials such as zinc oxide nanowires (Unsal and Bedeloglu, 2018). PENG works through coupling of piezoelectric and semiconducting materials in zinc oxide. When piezoelectric material is moved by mechanical motion, contact between two materials will show Schottky rectifying behavior. The Schottky barrier will store the piezoelectric charges and discharge it later, producing potential difference (Wang and Song, 2006).

Due to wide range of materials selection for the PENG, therefore it can be fabricated in different form and apply on various applications including act as wearable device. This is easily achievable by combining the inorganic materials proposed with flexible organic matrix such as polydimethylsiloxane (PDMS), polyvinylidene fluoride (PVDF) and silicone rubber (Zhao et al., 2021). However, the PENG are having a limitations which is high possibility of properties mismatching between piezoelectric fibre and the selected material which would lead to deflection of the model (Wan et al.).

2.3 Introduction to Triboelectric Nanogenerators

The idea of triboelectric nanogenerators (TENG) comes from figuring out how much mechanical energy was wasted in everyone's daily life. Charges induced during the triboelectric process are often regarded as negative effect in scientific research because electrostatic charges induced cause electronic breakdown and ignition. While looking from a different view, the electrostatic charges can be referred to as capacitive energy devices. Figure 2.5 is an equivalent circuit of TENG by Wu et al. (2019). The electrostatic charges induced on two contact and separated materials will promote electron flow while the materials are connected with a load. The electron will flow back and forth; thus it acts like an AC power source.

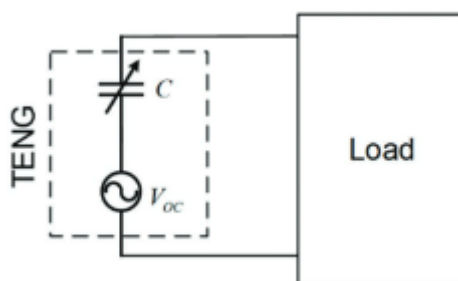


Figure 2.5: Equivalent Circuit Model of TENG (Wu et al., 2019).

According to Wang et al. (2015), TENG are operate based on the coupling of contact electrification and electrostatic induction. Triboelectrification or contact electrification can simply appear in two different materials with distinct triboelectric tendencies. When the two materials are in contact, or to be more specific which is have friction in between, the two materials will have an electric charge. In this condition, the materials will tend to achieve a balance charge by either sending electrons out or receiving electrons. Therefore, this imbalanced charge can be utilized by connecting them together with conducting wires and load to produce a channel for electron transfer. Electrostatic induction occurs when electrons flow through a circuit. The charges generated on the material surface can be held for a long time. In order to generate electricity, it serves as the induction source. Periodic motion causes the charges on the surface to change

periodically, resulting in continuously varying potential differences between electrodes attached to the materials.

The materials in contact for a TENG must be at least one dielectric material. To enable the transfer of electrons to create electrical potential, the electron must be transferred in conductors, thus dielectric materials need to have an electrode attached to their outer surface. On the other hand, if the material is conductive, then the material itself can be the electrode (Wang et al., 2015).

2.4 Working Modes of Triboelectric Nanogenerators

Currently, there are four basic modes of triboelectric nanogenerators, namely vertical contact separation mode, sliding mode, single electrode mode, and free-standing mode. The working mechanism and the pros and cons of each mode will be discussed in the following subsection.

2.4.1 Vertical Contact Separation Mode

The first triboelectric nanogenerators were invented by Fan et al. (2012) based on the vertical contact separation mode. The triboelectric materials used are Kapton, Polyethylene terephthalate (PET), and silver electrodes. The contact-separation mechanism is achieved by the bending motion as shown in Figure 2.6.

After pressing, the two materials get into contact, then the Kapton is negatively charged while PET is positively charged. Electron tends to move from an electrode of Kapton to an electrode of PET to achieve electrical equilibrium on both sides. Therefore, the electrode attaching to each of the materials is oppositely charged too. Upon release, the charged on the contact surfaces becomes least charged, thus electron flows back from the electrode of PET to the electrode of Kapton until it reaches electrical equilibrium. By repeating the bending and release motion, a continuous alternating current (AC) power supply can be achieved.

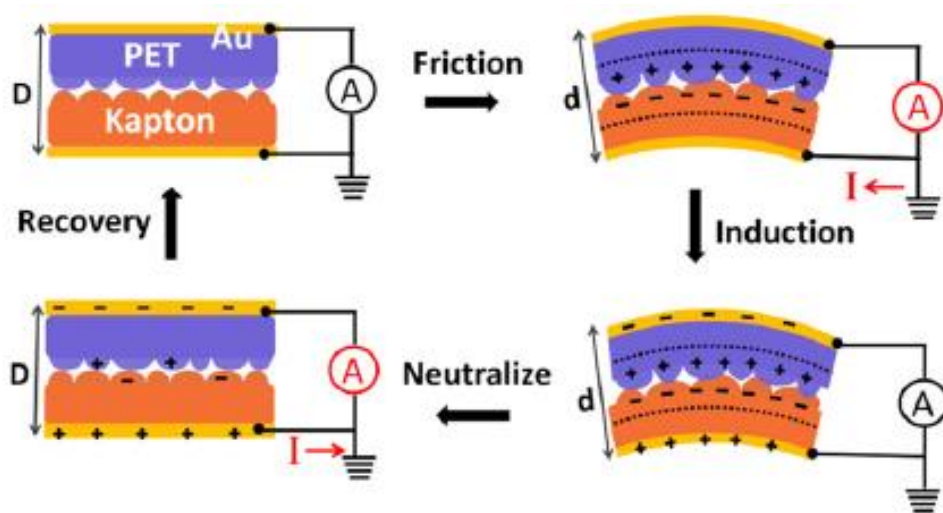


Figure 2.6: Contact Separation Mode TENG Mechanism (Fan et al., 2012).

Contact separation mode TENG is able to achieve high instantaneous power density while having the simplest structure design among the four modes of TENG. It can effectively harness short-distance continuous motion. However, for better performance of this mode of TENG, very effective switching between the contact and fully separated state is required. Therefore, a few structures, such as arch-shaped structures and spring-supported structures, have been developed (Wang et al., 2015).

2.4.2 Sliding Mode

Different from vertical contact separation mode, sliding mode generates charge through the motion of sliding two surfaces in lateral direction. Referring to Figure 2.7, contact electrification happens when the two materials are in a full contact state (Stage IV). When the two materials slide outwards, triboelectric charges are created, thus electron flow from the bottom electrode to the electrode on top until full separation of the two materials. When the material slides inwards, then the electron flow from the top electrode to the bottom electrode in order to balance the charge. Moving back and forth will then generates AC output (Wang et al., 2015).

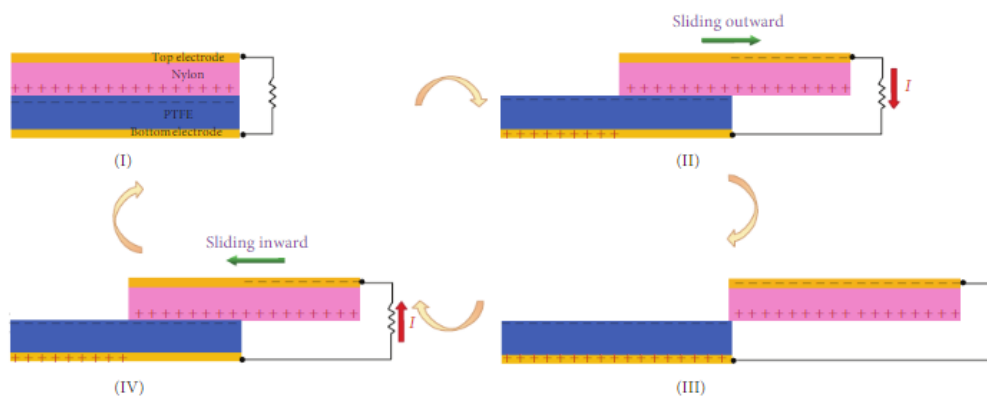


Figure 2.7: Sliding Mode TENG Mechanism (Lin et al., 2016).

Sliding mode TENG can be achieved with several structure such as planar motion, cylindrical motion, and disc rotation. Compared to contact separation mode, sliding mode has better energy conversion efficiency due to continuous contact of the two materials, where charges are generated as the materials are in contact for most of the time. Therefore, it is able to generate more output power (Lin et al., 2016). But, due to friction on the two contact surface during the sliding mode or rubbing, the sustainability of TENG in this mode will be relatively low. Therefore, most application prefer using contact separation mode.

2.4.3 Single Electrode Mode

The idea of single electrode mode is induced when researchers found out that it is very inconvenient to have all the materials attached to electrode. Wang et al. (2015) found out that moving objects will be naturally charged when in contact with air or other objects, therefore moving objects such as human skin or car tyres can be used as the triboelectric materials. Thus, if only one electrode is attached to a static material and connected to another electrode which will be used as reference or ground for electron transfer, the triboelectric mechanism can still be achieved. In this mode, the contact separation mode or sliding mode can be used with the same mechanism of the two mode. Figure 2.8 shows mechanism of single mode TENG.

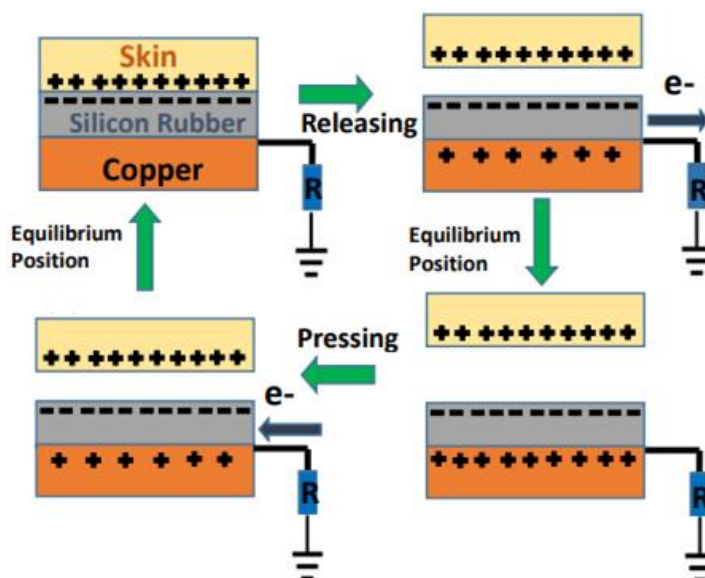


Figure 2.8: Single Electrode Mode TENG Mechanism (Khan et al., 2019).

The single electrode mode is less effective than the double electrode mode introduced previously because of the electrostatic screening effect (Wang et al., 2015). The charges can move freely as the reference electrode are not charged. Whereby the responses of single electrode mode TENG will be slower when used for a long time. However, due to the characteristics of not having an electrode on the other materials, therefore any electrically charged object can be used to generate the electric in single electrode mode.

2.4.4 Free Standing Mode

With further improvement from the single electrode mode, researchers find out another way to have any moving to trigger the triboelectric mechanism, namely the free standing mode TENG. As shown in Figure 2.9, a free-standing mode TENG proposed by Lin et al. (2016), two aluminium electrodes are connected to each other, while the dielectric materials, fluorinated ethylene propylene (FEP), will act as the moving object. The FEP contact with the left electrode causing the electrode to be positively charged. When the FEP is slide forward approaching the right electrode, causing the right electrode to be positively charged and the electron flows through the right electrode to the left electrode and achieve equilibrium. When it slides backward, the left electrode is then positively charged again, thus electron flow out from the left electrode. Thus, potential difference is generated.

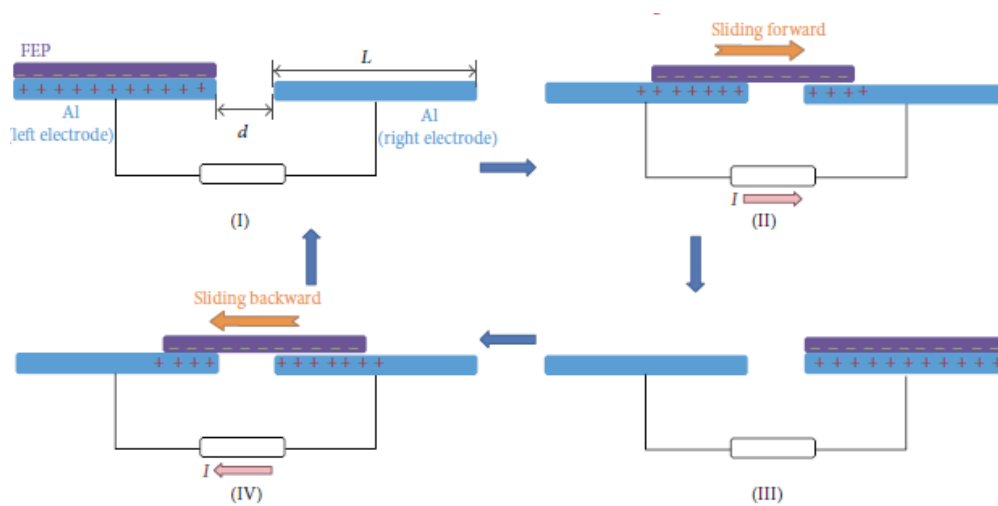


Figure 2.9: Mechanism of Free Standing Mode TENG (Lin et al., 2016).

Compared to the single electrode mode, it does not have screening effect, therefore it is able to transfer electrostatically induced electron more effectively and efficiently. There are variety of configuration of free standing mode. The example in Figure 2.9 is similar to the sliding mode, while the same mechanism with the material not contacting with the electrodes can be done as shown in Figure 2.10 (a). As this mode is capable in non-contact operation, an dielectric materials can be attach above the electrodes where it does not affect the operation of free standing mode TENG. In short, it has a very big benefit in long-term stability and sustainability because it avoids direct friction between two surfaces while giving good energy conversion efficiency (Wang et al., 2015).

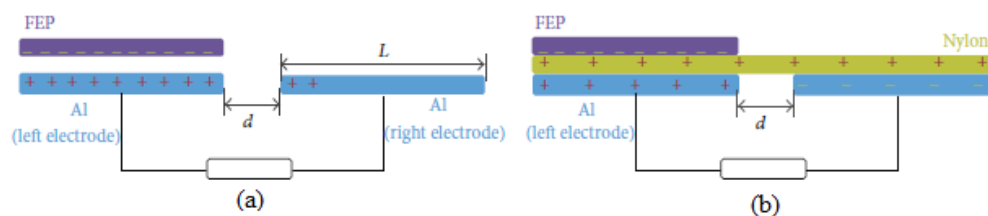


Figure 2.10: Free Standing Mode TENG with (a) Dielectric-conductor Configuration in Non-contact Sliding Mode. (b) Dielectric-dielectric Configuration (Lin et al., 2016).

2.5 Factors Affecting Performance of Triboelectric Nanogenerators

The performance of TENG are mainly based on the triboelectric materials used and the surface area of contact. Further studies found that humidity and temperature would bring slight impact on the output of TENG.

2.5.1 Choice of Materials

The triboelectric nanogenerators performance are strongly dependent on the materials surface charge density. Zhang and Olin (2020) did a research on materials used in TENG. Figure 2.11 is a statistics on fraction of materials often used as electron acceptors and electron donors from over 100 articles completed by them. From this statistics, it can be seen that the most frequently used materials include Polytetrafluoroethylene (PTFE), Polydimethylsiloxane (PDMS) and FEP for the electron acceptors and Aluminium (Al), Copper (Cu) and Skin for the electron donors. This can be explained with the triboelectric series as shown in Figure A-1 by Gooding and Kaufman (2011). The material at the top of the list is having strong tendency to create net positive charge when in contact with materials lower in the list, which means materials on top are good electron donors. In other way, materials at the bottom have high tendency to have net negative charge and are good electron acceptors. As the tendency of donating or accepting electrons is high, the ability of the material to store the charges is high, thus the surface charge density on the material after rubbing is high which means more electrons can be accepted or donated from that material. Therefore, comparing the statistics in Figure 2.11 and the triboelectric series, this explained that why are these are often used. PTFE has the highest tendency to accept electrons, therefore it is often used in TENG to obtain better performance.

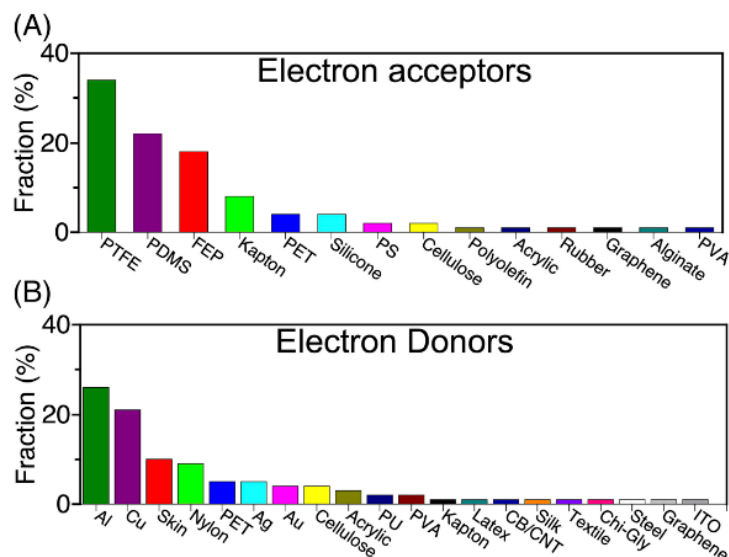


Figure 2.11: Statistics on Materials used in Fabricating TENG from 100 Articles. (A) Fraction of Electron Acceptors. (B) Fraction of Electron Donors (Zhang and Olin, 2020).

2.5.2 Surface Area of Contact

Surface area of the material contacting is one of the factor affecting the performance of TENG. Generally, larger surface area of contact would lead to higher output voltage. Therefore, various methods has been found by researcher to modify surface area of TENG to enhance performance.

Tcho et al. (2017) has compared two type of modification on TENG which is using dome and pillar array structure. Through simulation and experiment, it is found that dome is able to have more contact surface area compared to pillar when force is applied. Referring Figure 2.12, the reason that dome structure perform better is because the shape is easier to deform when pressed although the pillar array structure has larger surface area when calculated.

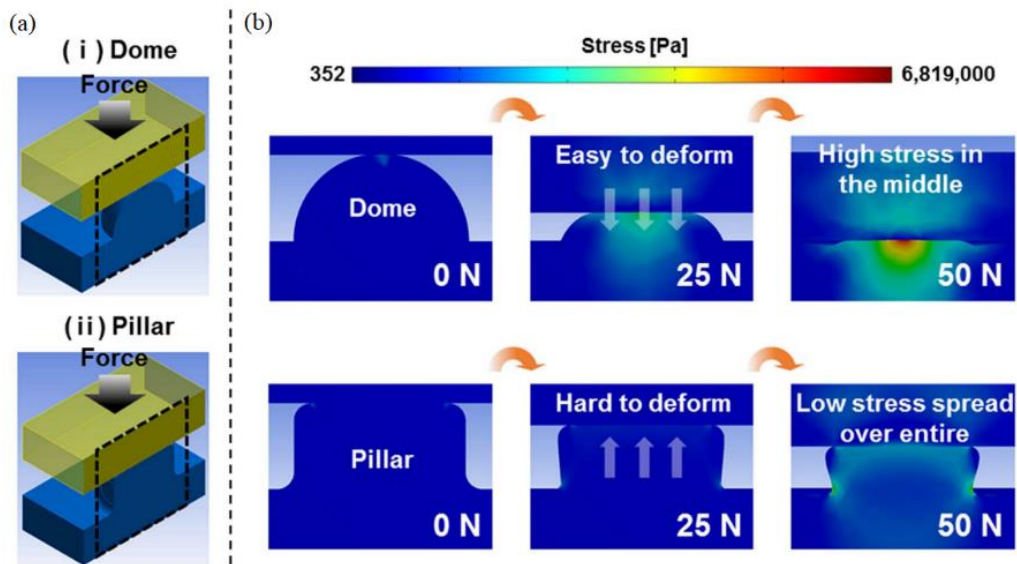


Figure 2.12: Simulation of TENG with Dome and Pillar Array Structure (Tcho et al., 2017).

Furthermore, Goh et al. (2021) proposed sponge based triboelectric nanogenerator (refer Figure 2.13) to improve the performance of TENG. The porous structure was done by adding sodium chloride particles into the eutectic gallium indium (EGaIn) Ecoflex mixture. The concept was to increase surface area of the material so that the charges can be trapped in the microporous structure of the material. The research has proven the theory with a result of charge difference increased by 50.8 % compared to the non-porous structure.

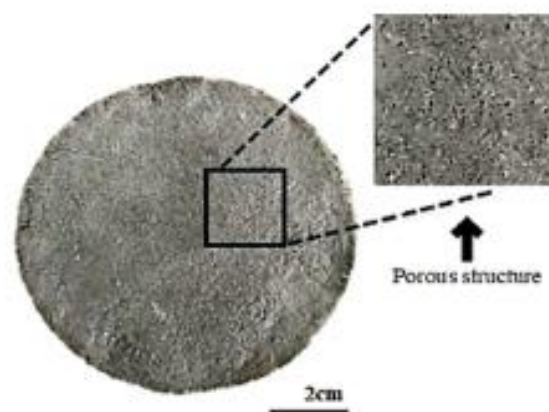


Figure 2.13: Sponge-based TENG (Goh et al., 2021)

Chung and Ke (2020) applied microneedle structure to enhance performance of TENG. Three kind of microneedle structure has been fabricated which are low density microneedle (LD-MN), high density microneedle (HD-MN), and overlapped microneedle (OL-MN) structure (refer Figure 2.14). The surface area are 17604.8 mm^2 , 19945.6 mm^2 and 22916.8 mm^2 respectively. The overlapped structure has generated voltage about 4 times of the low density microneedle structure. The researchers has compared their work with others, the overlapped structure generates the highest voltage.

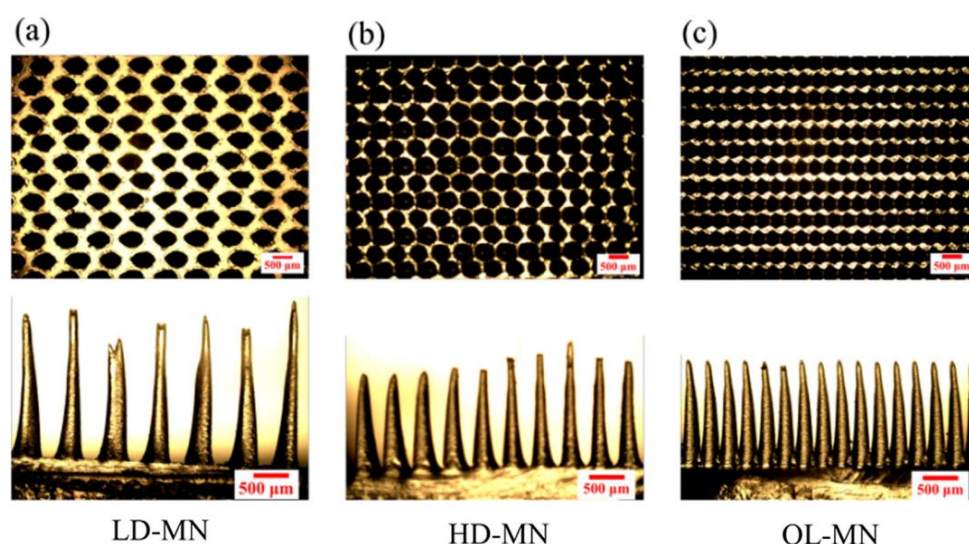


Figure 2.14: Optical Micrographs of TENG: (a) LD-MN, (b) HD-MN, and (c) OL-MN (Chung and Ke, 2020).

2.5.3 Humidity

According to Nguyen and Yang (2013), high humidity has unfavourable effect on the efficiency of contact electrification of dielectric materials. Their research found that when the humidity decreases, the charge generation between triboelectric materials increased up to 20%. While Shen et al. (2017) had proposed a TENG with resistance to humidity to overcome this effect. In their design, they introduced the electrospun nanofibrous membrane structure to eliminate the effects of water vapor on the electrical output of TENG. This finding is important especially for wearable device to be used on human during sports and also adapt to various environment.

2.5.4 Temperature

Temperature effect is important for application involving electronics in different places in the world. Various researcher found that environment temperature is influencing the performance of TENG. In Lu et al. (2017), when temperature increase from -20 to 150 °C, the performance of the TENG decreases. This is due to the ability of the material to store electron decreases. As temperature increases, the relative permittivity of material reduced. Therefore, Sun et al. (2019) has found out an material, ionogel to be used in TENG which is able to maintain its ability to store charge at various temperature and stable performance of the TENG.

2.6 Flexible Triboelectric Nanogenerators as Wearable Sensor for Human-machine Interaction

Skin is an excellent triboelectric materials which can act as the electron donors. According to Khandelwal et al. (2021), oily skin and dry skin have charge affinity of +45 nCJ⁻¹ and +30 nCJ⁻¹ respectively. Therefore, skin is often used as triboelectric materials for wearable sensor using TENG. To comply with skin, TENG needs to be flexible to act as a wearable sensor. The materials in contact with skin must be a good electron acceptors so that charge can be produce during contact separation of skin with the materials. This is to ensure seamless contact between skin and the sensor to acquire accurate result. Therefore, to achieve the flexible properties, flexible triboelectric materials recommended will be Polydimethylsiloxane (PDMS) and Ecoflex.

2.6.1 Polydimethylsiloxane (PDMS)

PDMS is one of the materials that are often used wearable self-powered sensor. This is due to its biocompatibility and elasticity that enable it to have full contact with soft and irregular surface such as human skin. Chen et al. (2018) presented a sensor patch for finger trajectory detection used in controlling robotic arm. It is a two-dimensional (2D) sensor patch made with PDMS with four electrodes output attached on wrist.

A self-powered finger motion sensor is developed by Dhakar et al. (2016). In this research, the finger motion sensor is developed according to the single electrode mode of TENG. The materials used includes gold, polyimide

and PDMS as shown in Figure 2.15. The gold act as the electrode. It has the PDMS layer fabricated with pyramid shape to increase the surface area of contact. The fabrication method is through molding. The contact electrification happens between the epidermis and PDMS. Thus, when the PDMS is negatively charged when moving away from the epidermis, the gold will be positively charged, thus sending out electron to ground. The polyimide layer act as electron storage or can said to be the capacitive system. The research analysed the signal when finger bend in different angle. The device developed is able to induce a peak voltage of 70V.

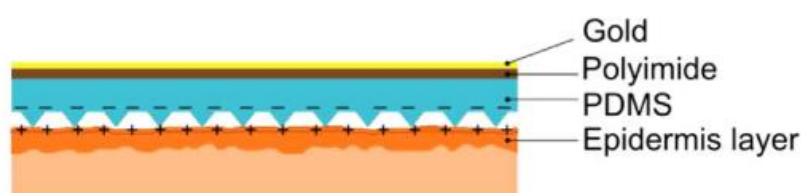


Figure 2.15: Schematic of Finger Motion Sensor by Dhakar et al. (2016).

There are several research made on tactile sensor. The tactile sensor developed by Yang et al. (2013) is the simplest one. The sensor created is based on single electrode mode, where the contact materials are PDMS and skin. Indium tin oxide (ITO) is used as the electrode. Contact electrification happened between skin and PDMS with micropyramid structures. The charge transfer happens between the ITO electrode and ground across a load. The tactile sensors are built in matrix form as shown in Figure 2.16 because the tactile sensors are built for touch pad technology. The sensors is able to track the location and pressure by touching. Their prototype is able to generate voltage up to 1000V.

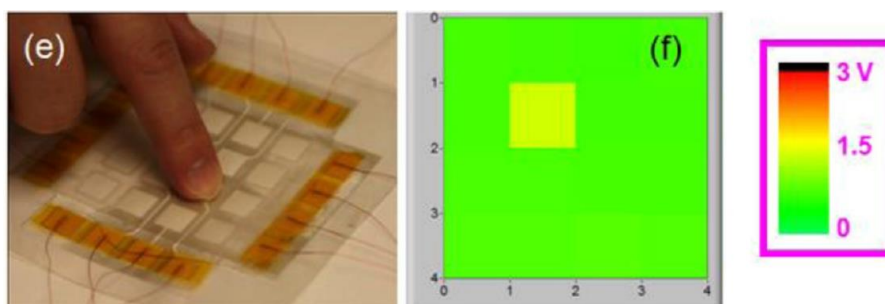


Figure 2.16: Self-powered Tactile Sensor in Matrix Form by (Yang et al., 2013).

Some research found that improvement can be made on PDMS to have better performance of TENG. Si et al. (2022) suggested mixing adequate amount of Polytetrafluoroethylene (PTFE) to improve the triboelectric properties of PDMS and applied it in a delta-parallel-inspired human-machine interface (DT-HMI). The sensor is used in control of virtual reality (VR) and augmented reality (AR) interactions. While He et al. (2020) suggested adding sufficient amount of conductive filler, MXene (titanium carbide, $Ti_3C_2T_x$). It helps to increase capacitance of TENG, thus improve surface charge density.

2.6.2 Ecoflex

Ecoflex is a platinum catalysed silicone rubbers. It has very strong, adhesive and stretchable characteristics. It can mount on human skin without causing discomfort and skin irritation due to its biocompatibility properties (Amjadi et al., 2015).

Anaya et al. (2020) had completed a research about eye motion sensor. In this research, a new configuration is proposed, namely non-attached electrode-dielectric triboelectric sensor. The configuration was designed by applying contact separation mode, with the electrode not attached to the dielectric materials. As addition, a single electrode mode is designed too as comparison to find the best design. The aim of this configuration is to generate voltage with non-contact electrostatic induction. Therefore, the sensor works based on interaction of two dielectrics material and the electric field generated. Figure 2.17 shows the prototype build and the placement of the sensor. When the muscle contracts, the materials are charged, thus allowing electron transfer. The materials used is Ecoflex and poly(3,4-ethylenedioxythiophene) polystyrene sulfonate (PEDOT:PSS). The size of the sensor is about $1.5\text{ cm} \times 0.6\text{ cm} \times 2\text{ mm}$. As the muscle contraction motion will only cause very small displacement, thus, they used conditioning circuit to amplify the signal. Without amplifying the output, the blinking eye motion can generate about 300 mV to 600 mV.

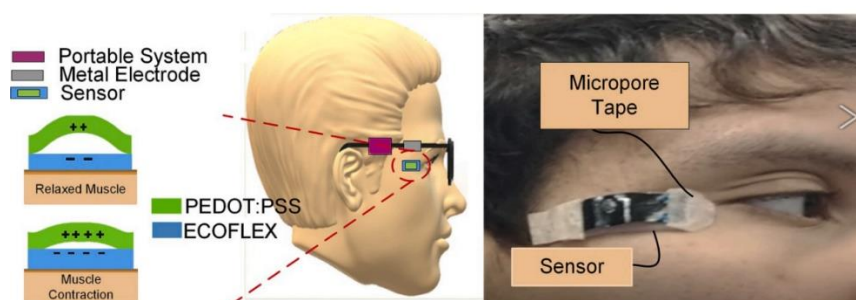


Figure 2.17: Orbicularis Oculi's Sensor Design and Placement. (Anaya et al., 2020)

Similar to PDMS, MXene has been introduced to use as liquid electrodes for TENG to amplify the performance (Cao et al., 2020). While another idea to enhance the TENG performance is by using electrolyte. Wang et al. (2021b) proposed using potassium iodide and glycerol as liquid electrode for the single electrode TENG made with Ecoflex. The electrolyte is injected into the middle cavity of the sensor. The sensor is able to generate output voltage of 300 V. The sensor was applied into several HMI such as control operation of LCD screen,

2.7 Summary

In this section, working theory and comparison of several self-powered mechanisms have been reviewed. Through comparison, it is found that triboelectric nanogenerators can achieve the best comfort experience as a wearable sensor due to a wide choice of materials selection. Therefore, flexible materials that comply with soft and irregular surfaces can be used in fabrication. Especially silicone rubbers such as PDMS and Ecoflex are showing excellent performance as triboelectric materials with human skin. While through reviewing different modes of TENG, single electrode mode and contact separation mode are found to have the simplest structure and mobility. Therefore, these two modes are simulated and tested in this project.

CHAPTER 3

METHODOLOGY AND WORK PLAN

3.1 Introduction

The project's materials and methodologies were covered in this chapter. The equipment used during prototype testing are also discussed. A simulation of the sensor design will be performed to aid in material selection, check on the sensor's behaviour, and determine the type of sensor with the best performance. The characteristics of TENG and its application will then be further studied through the fabrication of a prototype. With a better understanding of the prototype's behaviour after prototype testing, two applications for human-machine interactions are designed to demonstrate potential uses of the prototype.

3.2 Simulation of Self-powered Sensor

COMSOL Multiphysics is a simulation software supporting modelling designs and devices. It covers almost simulation packages for all engineering and physics fields, manufacturing, and scientific research. Modelling of design starting from 2D or 3D geometry design, characteristics of materials and physics phenomena can be done on this software while producing accurate results (I-STEM). In some journals, COMSOL Multiphysics is used to simulate TENG to obtain the potential difference from the motion. Therefore, this software is chosen to be used in this project. The modelling and simulation were completed by following tutorials from Teacheetah (2021) with some modifications based on self-expected results.

3.2.1 Contact Separation Mode

During the modelling pre-phase, 2D model is chosen because the motion to simulate is linear. The physics interface chosen is electrostatic which can be used to observe the potential and electric charge distribution.

First, an environment of 25 mm × 35 mm is created and defined as air. It will represent the environment in real world. A model as shown in Figure 3.1 is created where the size of human skin and PDMS are 5 mm × 1 mm, and

the electrodes' size are $5 \text{ mm} \times 0.1 \text{ mm}$. The width of the model is set to be 5 mm . The triboelectric charges density on the contact surface of PDMS and skin are assumed to be $-10 \text{ } \mu\text{C}/\text{m}^2$ and $+10 \text{ } \mu\text{C}/\text{m}^2$, respectively. The surface charge density value assumption was made based on simulation completed by Yang et al. (2013). While a resistor of $50 \text{ } \Omega$ is added to act as a load in the system. To demonstrate the motion of contact separation, the PDMS layer is moving upwards for 1 mm each time until it reaches 20 mm . Electric potential on both electrodes is tabulated in Microsoft Excel. The potential differences are calculated using Microsoft Excel and plotted. The simulation is repeated using Ecoflex to replace PDMS and silver to replace copper to find out materials that provide better outcome.



Figure 3.1: Schematic Diagram of Simulation Model for Contact Separation Mode.

3.2.2 Single Electrode Mode

The pre-phase setup for single electrode mode is the same as previous model. A model as shown in Figure 3.2 is created with human skin and PDMS size of $5 \text{ mm} \times 1 \text{ mm}$ and electrodes size of $5 \text{ mm} \times 0.1 \text{ mm}$. the bottom electrode act as a reference electrode to allow the electron flow between the two materials. The width of the model is set to be 5 mm . The triboelectric charges density on the contact surface of PDMS and skin are assumed to be $-10 \text{ } \mu\text{C}/\text{m}^2$ and $+10 \text{ } \mu\text{C}/\text{m}^2$, respectively. A resistor of $50 \text{ } \Omega$ is added to act as a load in the system. To demonstrate the motion of contact separation, the human skin layer is moving upwards for 1 mm each time until it reaches 20 mm . Potential difference can be obtained directly from the software thus it is tabulated and plotted. The simulation is repeated using Ecoflex to replace PDMS and silver to replace copper as manipulating variable.



Figure 3.2: Schematic Diagram of Simulation Model for Single Electrode Mode.

Additionally, after observing the results obtained, the environment is extended to $25 \text{ mm} \times 75 \text{ mm}$ and the human skin layer is moving upwards for 2 mm each time until it reaches 60 mm. This is to observe the potential difference when the distance is few times away from the previous setting due to exponential behaviour of the graph plotted. The result is tabulated and plotted.

3.3 Fabrication of Self-powered Sensor

The prototype is completed with the easiest way which is by molding method. This is to satisfy the properties of Ecoflex Solution which is initially in liquid state. The method at the same time is the most economical way to fabricate the prototype.

3.3.1 Materials

The triboelectric materials to be used in the self-powered is the Ecoflex 00-50 and it is purchased from Smooth-On. While the other contact materials will be skin. Copper sheets are used as the electrode which is accessible in the university. Furthermore, Polylactic Acid (PLA) filaments are used in 3D printing for the molds. The project is using 3D printing services provided by the university.

3.3.2 Conceptual Design

The mode of sensor chosen is single electrode mode as skin is chosen as the other contact material. The sensor is a simple rectangular and thin silicone rubber with a copper sheet as the middle layer with part of it outside the silicone rubber. The prototype is designed with Ecoflex with the size of 115 mm \times 32 mm \times 4 mm and a copper sheet with a size of 120 mm \times 28 mm \times 0.02mm. The conceptual design can be seen in Figure 3.3 which is completed using Solidworks.

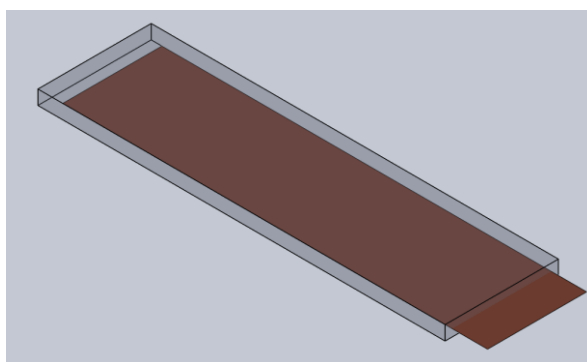


Figure 3.3: Conceptual Design of the Self-powered Sensor.

3.3.3 Fabrication Process

The process begins with designing the mold. Figure 3.4(a) shows the engineering drawing with the dimensions of the molds created using Solidworks. The Solidworks file is saved to a stereolithography (STL) file and send for 3D printing. The 3D-printed mold can be seen in Figure 3.4(b).



Figure 3.4: Molds created using Solidworks and 3D printed.

Next, Ecoflex solution is prepared. The Ecoflex 00-50 consist of 2 solutions: Part A and Part B as shown in Figure 3.5. Each solution of weight 10 g is prepared. The solution is mixed in a ratio of 1:1 and stirred slowly to prevent too much entry of air bubbles. Then, the mixture solution is poured into the mold up to about 2mm thickness of the prototype. The copper sheet is cut into sizes of 120 mm \times 28 mm and placed on top of the mixture solution. Lastly, pour the mixture solution again to cover the copper sheet. The prototype is set aside to cure under room temperature. Figure 3.6 shows the process of molding the prototype. The prototype is dispatched from the mold when fully cured and the prototype is completed. Figure 3.7 shows the final prototype.



Figure 3.5: Ecoflex 00-50 Solution.

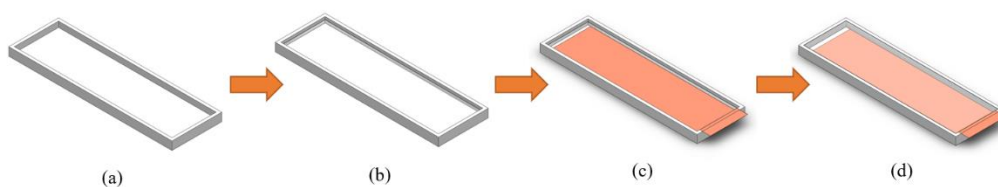


Figure 3.6: Molding Process of the Self-powered Sensor.



Figure 3.7: Self-powered Sensor Fabricated.

3.4 Characterization of the Self-powered Sensor

The characterization of the sensor is done by using NI ELVIS II+ (National Instrument, United States) board as shown in Figure 3.8. The purpose of using this equipment is to obtain and receive data in computers directly from the sensor for further analysis and further development of the application. The data from the sensor can be obtained by connecting the electrode to the Digital Multimeter (DMM) of the board. The measured data will be logged and displayed in a virtual interface, LabView NI.

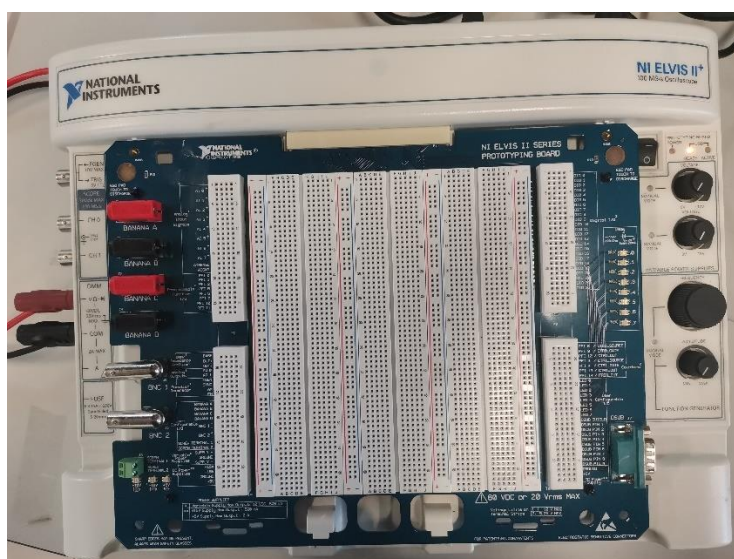


Figure 3.8: National Instrument (NI) ELVIS II+ Board.

In the circuit diagram (Figure 3.9), a voltage divider circuit is constructed and used when measuring the voltage generated by the sensor. The maximum voltage that can be read by the DMM of the NI Elvis II+ board is 10 V, where voltage exceeds the value may damage the device. Therefore, the voltage divider circuit is used to scope down the voltage to be read by the device. Equation 3.1 is an equation formed according to the voltage divider rule with a circuit of 2 resistors. R_2 should be a resistor of a lower value so that the voltage passing over the resistor is lower, whereby the voltage measurement, V_{out} , is made over R_2 . During data collection, $R_1 = 10\text{ M}\Omega$ and $R_2 = 50\text{ k}\Omega$ are used in the circuit. A very large value of R_1 is used to ensure that the voltage measured over R_2 will not exceed 10 V.

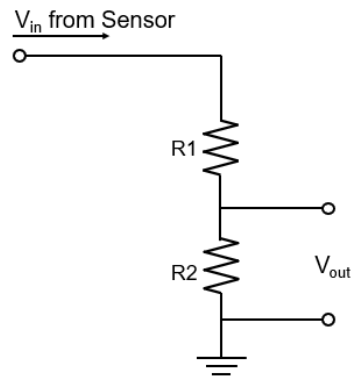


Figure 3.9: Voltage Divider Circuit used in Data Collection.

$$V_{in} = \frac{R1+R2}{R2} V_{out} \quad (3.1)$$

where

R = resistor value, Ω

V_{in} = voltage from sensor, V

V_{out} = output voltage to DMM, V

To obtain the data using LabVIEW, a block diagram as shown in Figure 3.10 is built. The voltage measurement is obtained by the DAQ Assistant and sent to the Waveform Chart for real-time observation of the graph of voltage over time. After a specific time span, The system is stopped and the data is collected and output to an excel file.

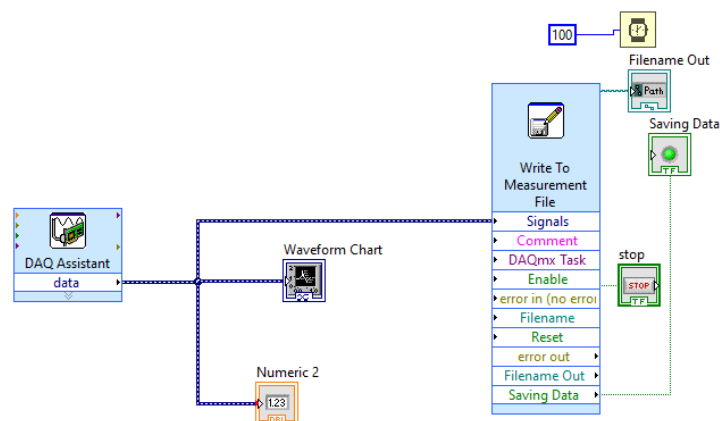


Figure 3.10: Block Diagram Built in LabVIEW.

3.5 Human-machine Interaction Applications of the Self-powered Sensor

There are a total of two HMI applications designed for the self-powered sensor as proof of principle. The applications are designed based on the characteristics of the self-powered sensor tested earlier on. The sensor is stuck on a human arm during a demonstration of the HMI applications. First, a ball bouncing application where a ball will bounce to a height based on the voltage value measured, which represents force applied on the sensor. Next, three LEDs of different colors are to be light up based on the frequency of hand tapping on a sensor.

The applications are designed using Arduino Uno R3 and MATLAB software with Arduino Add-Ons. The voltage divider circuit is also used when reading the voltage generated by the sensor with the Arduino Uno R3. This is because the maximum voltage readable by Arduino analog pin is 5V. The resistors value remain the same from the characterization of the sensor which is $R1 = 10 \text{ M}\Omega$ and $R2 = 50 \text{ k}\Omega$. The Arduino Uno R3 is connected to a computer.

3.5.1 Ball Bouncing Application

In this application, a ball will bounce based on the voltage value detected by the sensor. The environment is set to have a maximum height of 10, which represents 100 V. Therefore, any signal exceeding 100 V will cap the bouncing peak at the height of 10.

The connection of the sensor as input voltage (V_{in}), voltage divider circuit, and Arduino for the ball bouncing application can be seen in Figure 3.11. The circuit consists only of the voltage divider circuit because the applications are only required to receive signal and produce output in the computer. Voltage over $R2$ is measured using Arduino's analog pin, A0.

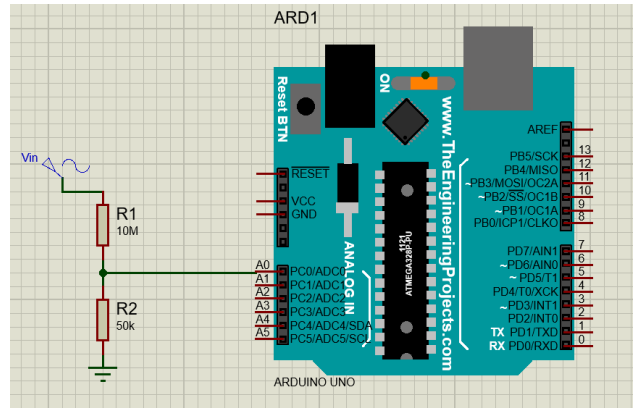


Figure 3.11: Circuit Diagram for Ball Bouncing Application.

The flowchart and code for this application can be found in Appendix B. Refer to the code, the application will continuously read the voltage from the analog pin, A0. A threshold is set because there are noises while reading the voltage from Arduino. If the voltage exceeds the threshold set, 12 V, the ball will bounce.

The equations of uniform acceleration are used to enable the ball to bounce with gravity. The initial velocity was obtained by Equation 3.2 where the final velocity is the velocity when the ball is at peak, which equals zero velocity, acceleration is the gravity, -9.81 m/s^2 , and distance is the peak height that the ball should bounce to. The total time for the ball to bounce is calculated using Equation 3.3. In this case, when the ball reaches the “floor” the distance is 0, while the initial velocity is the velocity calculated previously. With the information calculated, a loop to calculate the position of the ball every 0.01 s can be created. The velocity is updated using Equation 3.4 while position is updated using Equation 3.3. For the case where voltage exceeds 100 V, the velocity will not be 0 m/s when it reaches the peak height at 10, therefore, it is coded to equal to 0 m/s. The ball will continue falling after that. The ball will stop bouncing when it reaches the “floor” and wait for the next signal.

$$v^2 = u^2 + 2as \quad (3.2)$$

$$s = ut + \frac{1}{2}at^2 \quad (3.3)$$

$$v = u + at \quad (3.4)$$

where

v = final velocity, m/s

u = initial velocity, m/s

a = acceleration, m/s^2

s = distance, m

t = time, s

3.5.2 Turn On LED Application

This application used the frequency of signal detected within 4s and signal voltage exceeding a threshold of 12V to trigger the LED on. The red LED should be on when there is 1 signal, the yellow LED should be on when there are 2 signals and the green LED should be on when there are 3 or more signals. All the LEDs should be off when there is no signal. A graph showing the real-time signal is plotted too.

The connection of the sensor as input voltage (V_{in}), voltage divider circuit, and Arduino for the ball bouncing application can be seen in Figure 3.12. The circuit is almost the same as the previous application where voltage over R2 is measured using Arduino's analog pin, A0, but 3 LEDs of different colors (red, yellow, and green) with resistors of 10 k Ω are connected to pin 9 to 11. The flowchart and code for this application can be found in Appendix C. The application will continuously read the voltage from the analog pin, A0, and update the graph. A threshold the same as the previous application is set. If the voltage does not exceed the threshold, the graph will not show the signal.

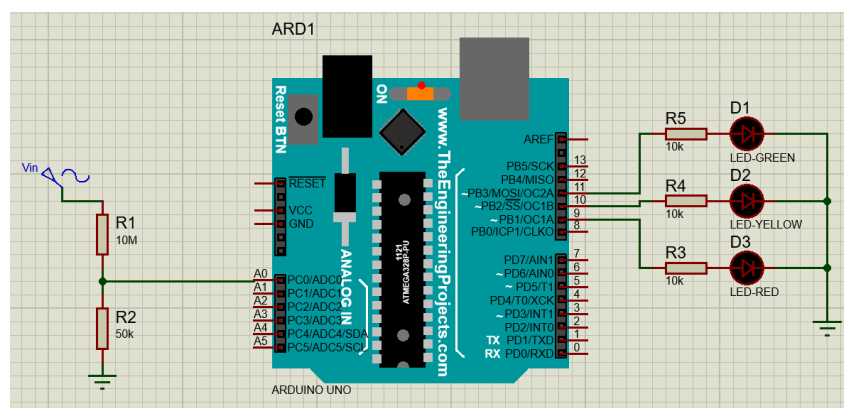


Figure 3.12: Circuit Diagram for Turn on LED Application.

3.6 Summary

In short, a simulation of the self-powered sensor has been completed. Contact separation mode and single electrode mode triboelectric nanogenerator have been simulated with Ecoflex and PDMS as the manipulating contact materials and copper and silver as the manipulating electrode materials. After that, the Ecoflex and copper electrodes has been chosen as the final material for the prototype. The prototype was completed using the molding method, where the mold was designed using Solidworks and 3D printed. Furthermore, the sensor was characterized using the NI Elvis II+ board and LabVIEW software with the voltage divider circuit. Last but not least, two applications were designed based on the characteristics of the sensor. This is done by using Arduino Uno R3 and MATLAB software.

CHAPTER 4

RESULTS AND DISCUSSION

4.1 Introduction

This chapter first discussed the results obtained from the simulation conducted. The result will mainly compare the difference in the output provided by the two different modes of TENG, by different triboelectric materials and electrodes, and observe the behavior of the potential difference when distance increases. Next, the characterization of the self-powered sensor is completed. The characteristics of the signal. The results of voltage over force and voltage over frequency are analyzed. Lastly, two applications for human-machine interaction with the self-powered sensor are reviewed and the results can be found in the following chapter.

4.2 Simulation

Simulation of TENG with different triboelectric materials and electrodes is completed. The simulation has been done on two modes of TENG which are the contact separation mode and the single electrode mode. The same setting of environment, size of materials, and size of electrodes are provided.

Figure 4.1 shows the distribution of electric potential generated from the simulation of the contact separation mode of TENG. From the figure, it is found that the electric potential generated on the two electrodes of each material increases as the moving materials move further. This is due to more electron losses accepted during the motion. Table D-1, Table D-2, and Table D-3 show the electric potential obtained from COMSOL Multiphysics and the potential difference obtained by finding the difference between the electric potential in the two electrodes. The potential difference is the difference between the electric potential of the bottom electrode and the top electrode. Table D-4 compiled the potential difference for all materials and electrodes. The result is plotted in Figure 4.2. From the graph, it can be seen that the potential difference has not much difference when the materials and electrodes are changed. For contact separation mode TENG, around 4.5 kV can be generated when the distance reaches 20 mm.

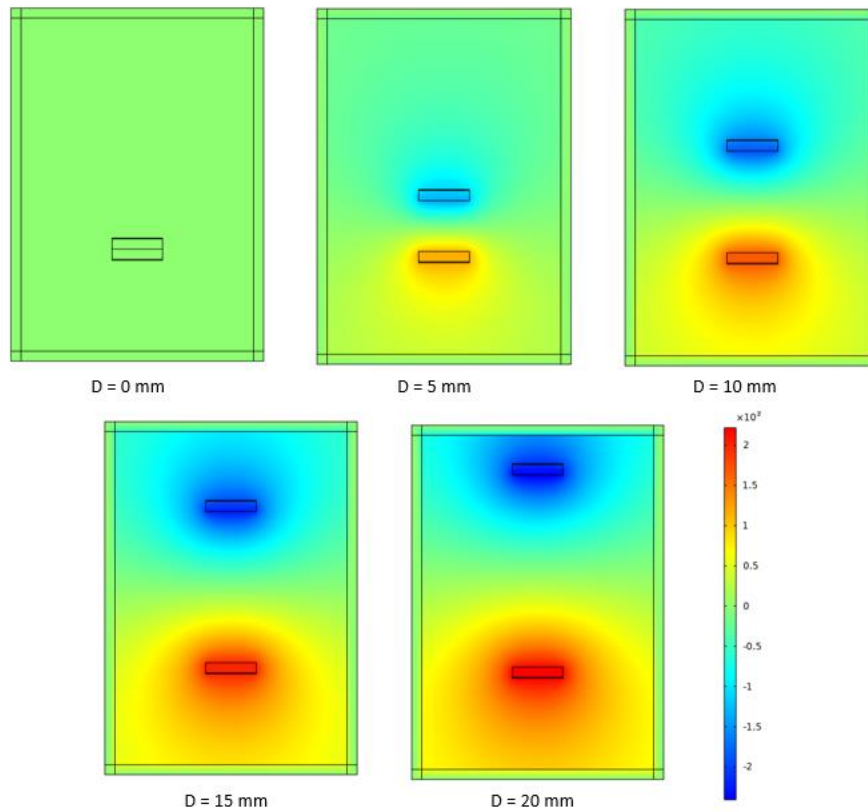


Figure 4.1: Electric Potential Distribution for Simulation of TENG in Contact Separation Mode when Distance (D) between the Contact Surface of Elastomer and Skin Increases.

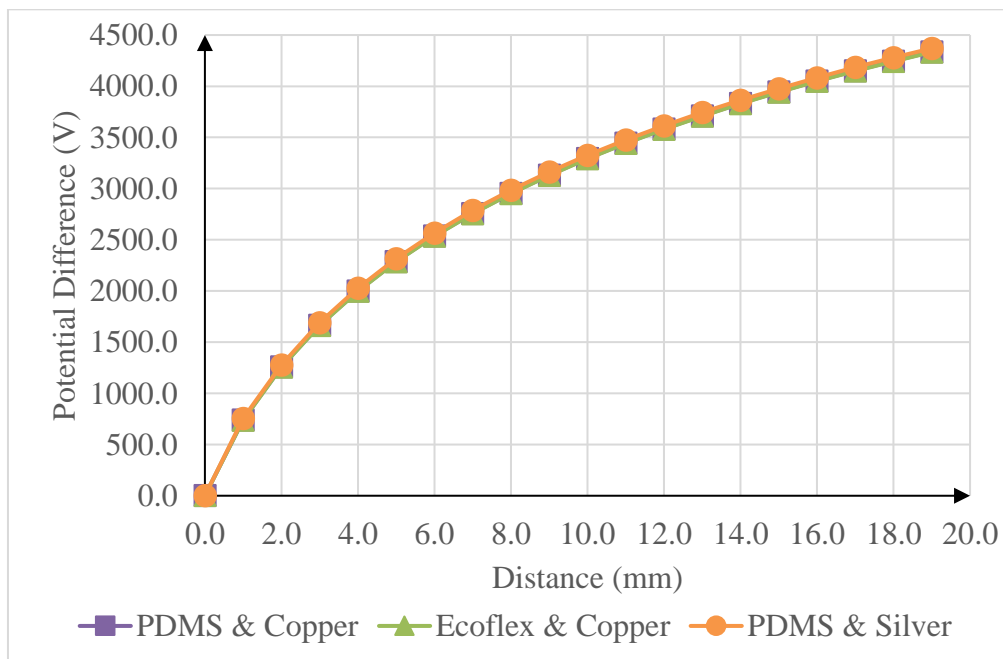


Figure 4.2: Graph of Distance against Potential Difference for Simulation of TENG in Contact Separation Mode.

Figure 4.3 shows the distribution of electric potential generated from the simulation of the single electrode mode of TENG. The electric potential generated on the two electrodes of each material increases as the moving materials move further as seen in the figure. This is due to more electron losses accepted during the motion. Table D-5 shows the potential difference obtained from the simulation and the results are plotted in Figure 4.4. The potential difference is results generated directly from COMSOL Multiphysics. The potential differences are similar when different materials and electrodes are used, where all of them can generate around 150 V when the distance reaches 20 mm.

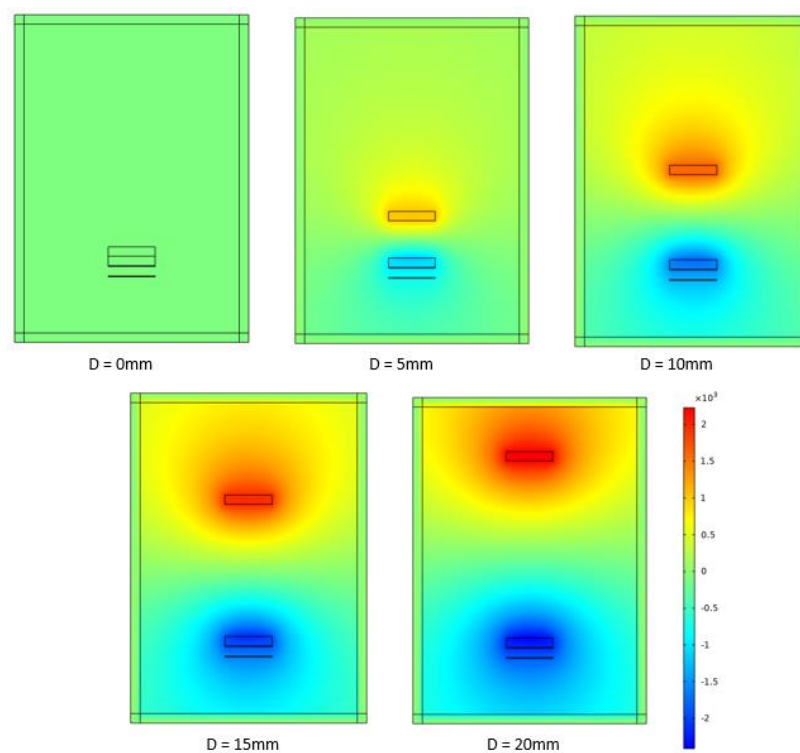


Figure 4.3: Electric Potential Distribution for Simulation of TENG in Single Electrode Mode when Distance (D) between the Contact Surface of Elastomer and Skin Increases.

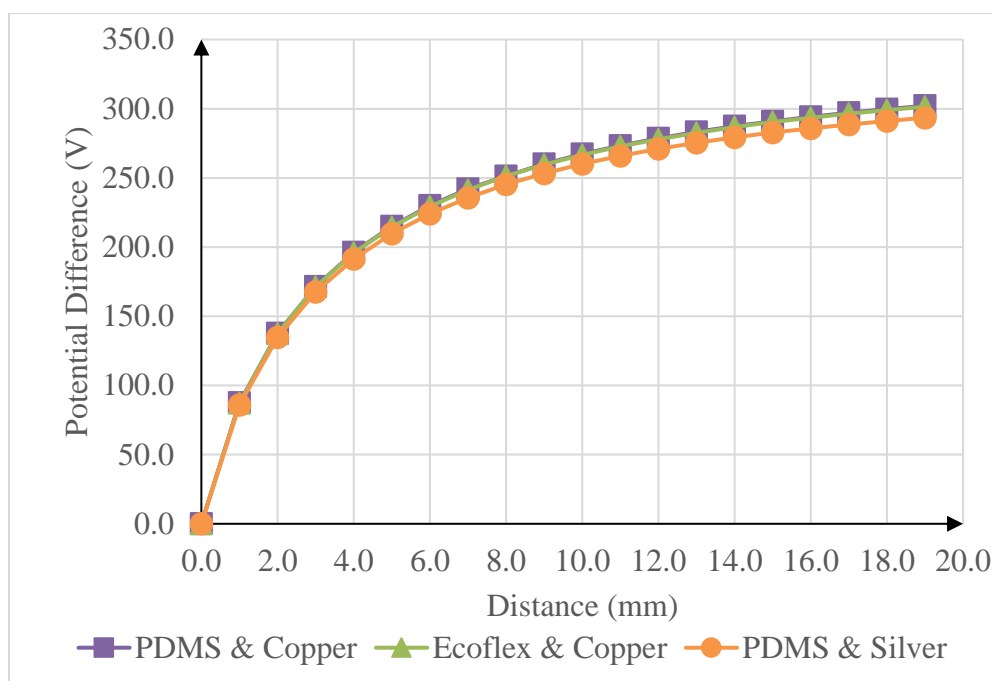


Figure 4.4: Graph of Distance against Potential Difference for Simulation of TENG in Single Electrode Mode.

The potential difference in both modes increases exponentially when the distance between the contact surface of PDMS and skin increases. Comparing the results in the two modes of TENG, it is obvious that the contact separation mode is generating relatively higher voltage when the moving materials move to the same distance in both modes.

Due to the exponential behavior of the outcome, another simulation is carried out to further prove the exponential behavior of the potential difference when distance is increased. This result is shown in Table D-6 and Figure 4.5. The result has proven that the potential difference generated by TENG will cap at a certain value when it reaches a certain distance. This is due to the net electric charge has achieved. Thus, no more electrons can be sent out to generate power. This also represents the peak potential difference that can be generated by the sensor. With this information, optimization of development of TENG can be done.

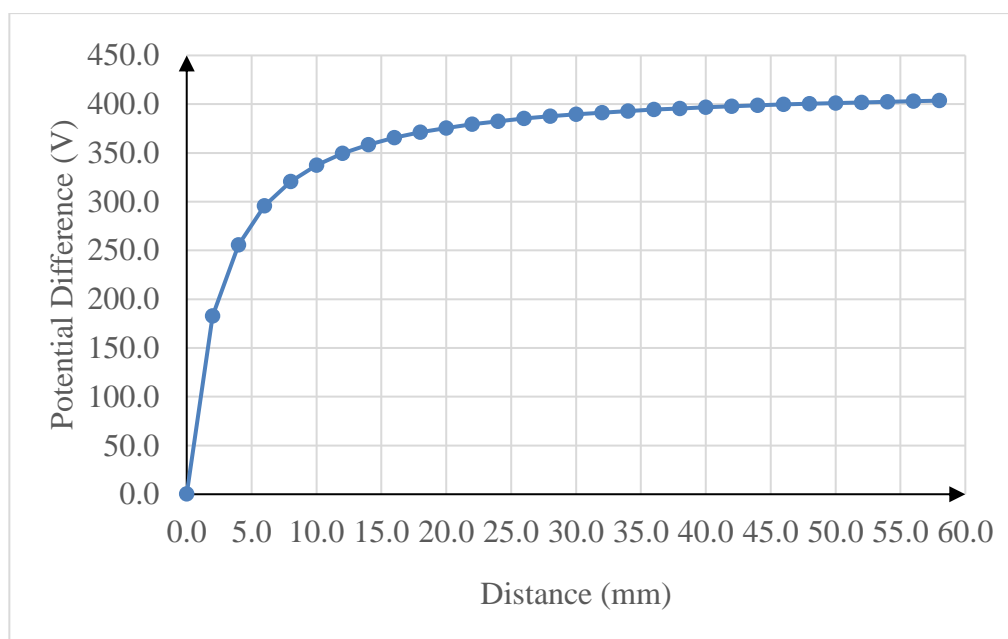


Figure 4.5: Graph of Distance against Potential Difference for Simulation of TENG in Single Electrode Mode for Distance up to 60 mm.

4.3 Characterization

First, the characterization of the signal produced by a self-powered sensor is observed. The signal produced by one tap from the hand on the sensor can be seen in Figure 4.6. When the hand is in contact with the Ecoflex surface, the Ecoflex surface will become negatively charged. Thus, once the hand is released from the sensor surface, the copper electrode will release electrons so that it can be positively charged and reach an equilibrium state with the Ecoflex (refer to Figure 4.7 (ii)). The electrons pass through the resistor and go to the ground producing a positive potential difference between the resistor. The copper electrode stop releasing electrons when the copper electrode and Ecoflex are in an equilibrium state which means the contact surface of both of the materials are not charged (refer Figure 4.7 (iii)). After that, the signal drops to negative potential difference as the electrode itself recharges back to equilibrium (refer to Figure 4.7 (iv)).

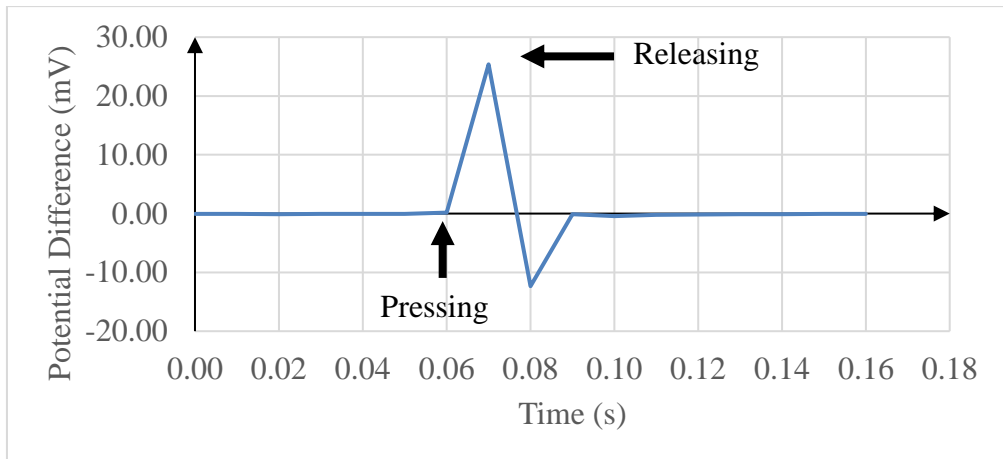


Figure 4.6: Sensor Output during Pressing and Releasing.

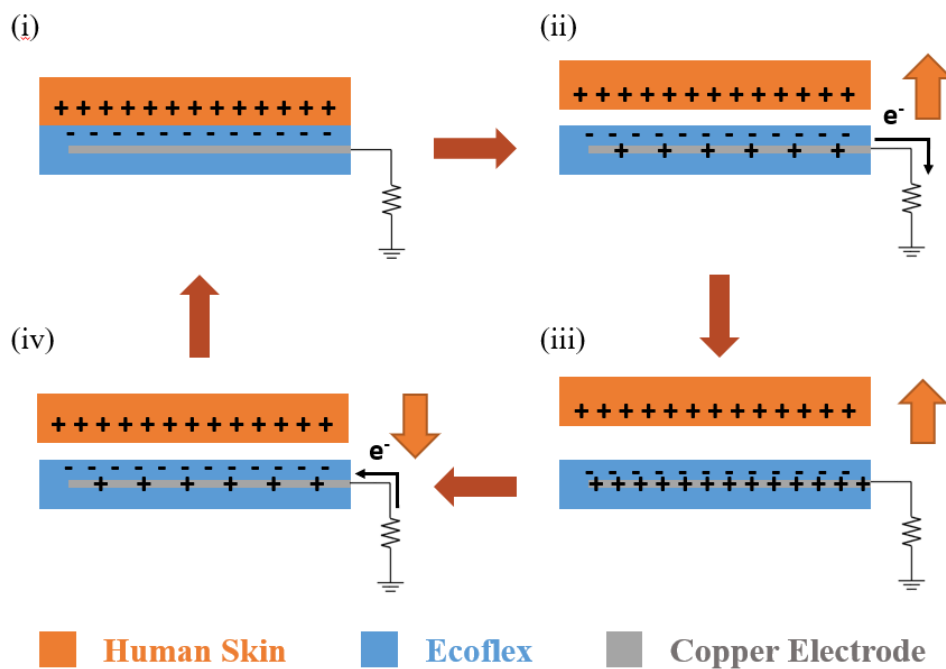


Figure 4.7: Working Mechanism of Self-powered Sensor.

Furthermore, the signal generated by continuous tapping on the sensor can be observed in Figure 4.8. The sensor is able to generate a signal approximate range of -500 mV to 700 mV. Mostly, the first few taps would generate lower potential differences and increase slowly. At a certain point, the voltage would drop to a very low value again. This is due to the characteristics of single electrode mode TENG whereby it takes a longer time to recharge. This can also be seen as there are very large negative signals sometimes, which is due to the sensor are not fully recharged. Therefore, the

triboelectric mechanism works in the opposite way which attracts the electron back. As can be seen in this figure, the potential difference is difficult to control to maintain at the value because very small charges different during tapping would make different potential differences generated.

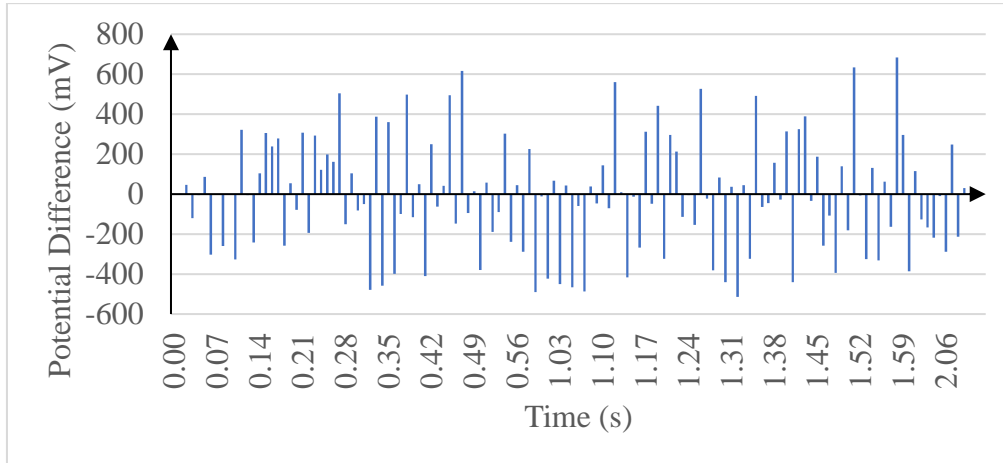


Figure 4.8: Signal Output when Continuous Tapping from Hand on Sensor.

Besides the effect of force applied towards the potential difference is observed. The result is shown in Figure 4.9. From the graph, it can be seen that the potential difference generated is higher as the force applied increased. This is due to the higher force applied during contact will produce more charges and therefore more electrons are sent out from the copper electrode which results in a higher potential difference.

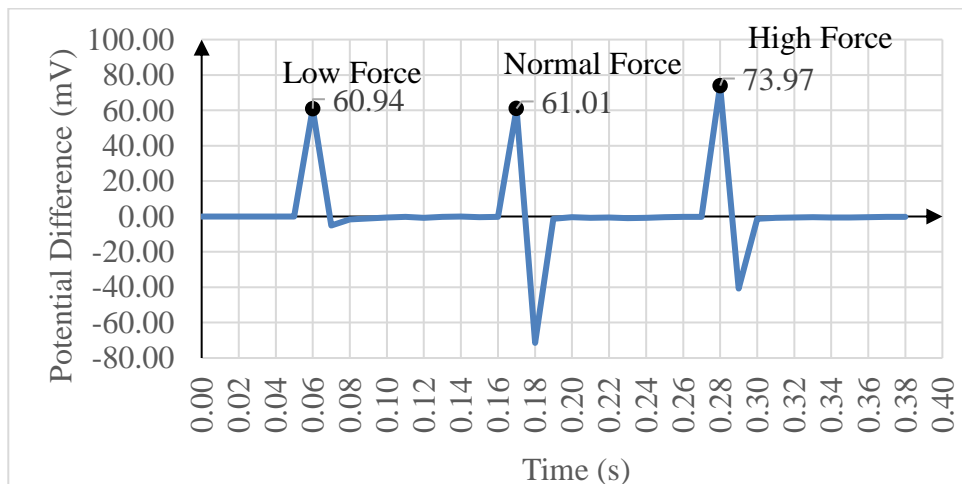


Figure 4.9: Signal Output when Tapped with Different Force on Sensor.

The effect of frequency on the potential difference can be found in Figure 4.10. Each colored area represents the time frame considered when capturing the signals based on frequency. The 1st area represents tapping the sensor 1 time, the 2nd represents 2 times, and the 3rd area represents 3 times. The results have proven that the sensor is able to capture the frequency of tapping accurately. The result was supposed to be able to show that when the frequency of tapping is higher, the potential difference will be higher. Due to the sampling rate of the NI Elvis II+ board that causes the peak obtained might not be very accurate and the human hand cannot apply very consistent force on the device. Thus, the theory cannot be applied in this case.

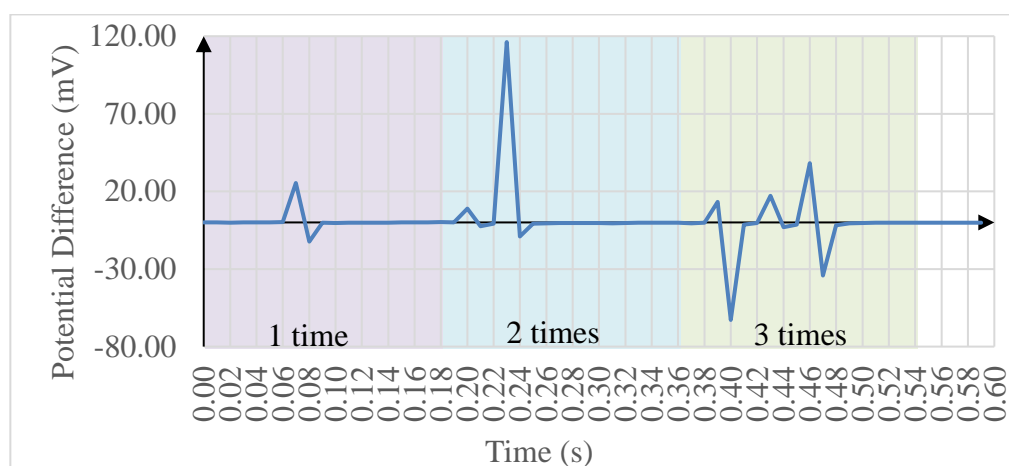


Figure 4.10: Signal Output when Tapped with Different Frequency on Sensor within a Specified Time Frame.

4.4 Human-machine Interaction Applications

The first application is designed based on the effect of force on the self-powered sensor. The application is able to read the voltage generated by the sensor and output as desired. The outcome can be found in Figure 4.11. When the voltage is 18.6657 mV, the ball is able to bounce to a peak of 1.8666 cm and it is the same for other input voltages. When the ball bounces, it is also showing a gravity effect where the velocity decreases when going up and increases when falling down so that it looks smoother.

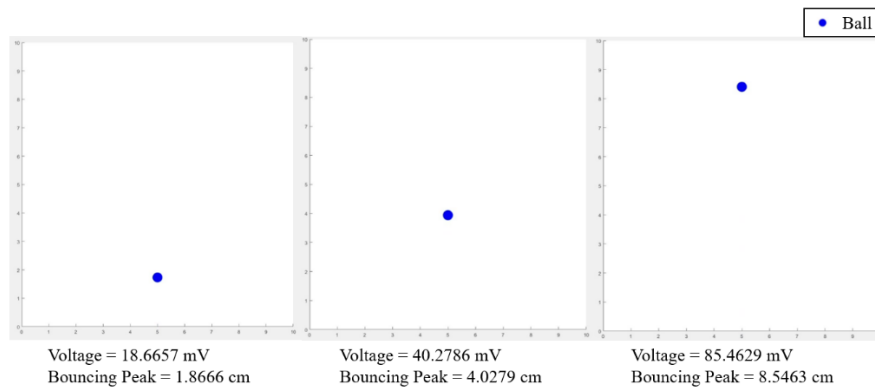


Figure 4.11: Outcome of Ball Bouncing Application.

Next, in the turn-on LED application, the algorithm was designed based on the frequency of tapping in the specific time frame. Referring to Figure 4.12 (a), there is no LED lighting up because there are no signal given. While the red LED is turned on when one tap is applied on the sensor as in Figure 4.12 (b). The yellow LED is turned on when hand tapped 2 times on the sensor as shown in Figure 4.12 (c). Lastly, green LED is turned on when the sensor is being tapped for 3 times (Figure 4.12 (d)) and more (Figure 4.12 (e)). The application is able to read the frequency of the signal accurately and do the desired action based on the signal given.

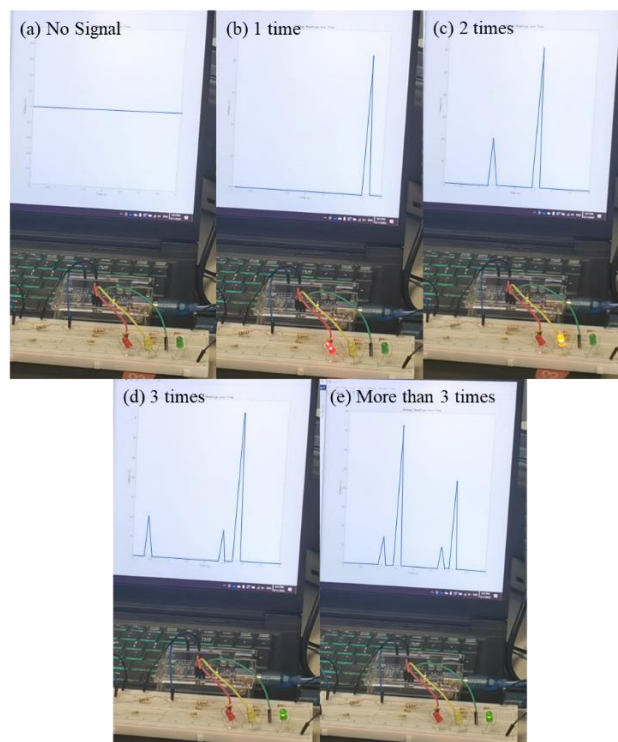


Figure 4.12: Outcome of Turn On LED Application.

4.5 Summary

According to the simulation results obtained, contact separation mode (4.5 kV) is able to generate higher voltage than single electrode mode (150 V). However, it is impossible to have a contact separation mode self-powered sensor with skin as one of the materials because it is impossible to attach electrodes to the skin. Therefore, a single electrode mode has been chosen to be used in the sensor. The materials and electrodes chosen to be the manipulating variables have not had much effect on the performance of TENG. The potential difference increased exponentially to the distance between the contact surfaces of the two materials. The potential difference will cap at a certain value when reaching a certain distance.

From the characterization of the self-powered sensor, the positive peak and negative peak are analyzed. As the sensor is a single-electrode TENG, therefore sometimes the electron needs sometimes to return to the copper electrode. The sensor is able to generate a signal approximate range of -500 mV to 700 mV. It is found that when force is greater, the potential difference generated is greater. Furthermore, it has been proven that the sensor is able to read the frequency of tapping in a specific time span accurately.

After that, the characteristics are applied to two human-machine interactions. In the ball bouncing application, the ball is able to bounce based on the force applied on the sensor; whereas in the turn-on LED application, the sensor captured the frequency of tapping and lights up the desired preset LED.

CHAPTER 5

CONCLUSIONS AND RECOMMENDATIONS

5.1 Conclusions

In the project, a wearable self-powered sensor is successfully fabricated. First, a simulation is done to study the outcome of different modes of triboelectric nanogenerators, and the effects of different materials used when in contact with skin. The outcome from that, Ecoflex is chosen as the contact material while copper is the electrode.

After that, the final sensor is designed in a rectangular shape with dimensions of 115 mm × 32 mm × 4 mm and a copper sheet as the electrode. Through characterization of the sensor, it has proven to be able to generate a signal with voltage in the range of approximately -500 mV to 700 mV. Moreover, the sensor has also shown increasing voltage when a greater force is applied while tapping it with a hand. The sensor is also able to capture the frequency of tapping accurately.

With the characteristics of the self-powered sensor, two human-machine interaction applications are designed and work as expected. The first application is the ball bouncing application where the ball is able to bounce up based on the force applied to the sensor. The other application is the turn-on LED application. The sensor is able to capture the frequency tapped on the sensor and light up the desired LED.

5.2 Recommendations for Future Work

The proposed sensor has proven its ability to attach to human skin and be applied to several HMI applications. However, the electrode chosen is copper, which is solid and rigid and will break when used in long term and stretch exceeding its strength limit. Therefore, future work can be done on replacing it with stretchable electrodes as suggested by Wen (2020). The three methods include the prestrain-coating-release method, embedding conductive materials into elastomer, and fundamentally stretchable electrodes such as liquid-state electrodes and conductive gel.

Furthermore, the proposed prototype can work independently as it does not need power sources, but it still has to connect to a processor to be applied in an application. Thus, it has caused issues in mobility as a wearable device because the processor still needs a bulky power source and connection to a computer for operation. The recommendation to solve the solution is to treat the TENG as the energy harvester and connected it to a capacitor. With proper design with energy harvesting characteristics to increase the power supply provided by TENG and the selection of suitable microprocessors, the devices could be more portable and comfortable as wearable devices. Furthermore, a Bluetooth module or another wireless transceiver can be implemented so that signals can be sent to computer or mobile phones for further applications.

The current application is simple as the sensor is single output which limits the possible application that can be developed and used. Therefore, the tactile structure makes it a 2D structure and can be used to improve this limitation. More signals will allow users to do more human-machine interaction. While implementing machine learning would be an advantage to make it applicable in more applications and have more human-machine interaction.

REFERENCES

- Amjadi, M., Yoon, Y. J. & Park, I. 2015. Ultra-stretchable and skin-mountable strain sensors using carbon nanotubes–Ecoflex nanocomposites. *Nanotechnology*, 26, 375501.
- Anaya, D. V., He, T., Lee, C. & Yuce, M. R. 2020. Self-powered eye motion sensor based on triboelectric interaction and near-field electrostatic induction for wearable assistive technologies. *Nano Energy*, 72, 104675.
- Bandodkar, A. J. & Wang, J. 2016. Wearable biofuel cells: a review. *Electroanalysis*, 28, 1188-1200.
- Cao, W. T., Ouyang, H., Xin, W., Chao, S., Ma, C., Li, Z., Chen, F. & Ma, M. G. 2020. A stretchable highoutput triboelectric nanogenerator improved by MXene liquid electrode with high electronegativity. *Advanced Functional Materials*, 30, 2004181.
- Chen, T., Shi, Q., Zhu, M., He, T., Sun, L., Yang, L. & Lee, C. 2018. Triboelectric self-powered wearable flexible patch as 3D motion control interface for robotic manipulator. *ACS nano*, 12, 11561-11571.
- Chung, C. & Ke, K. 2020. High contact surface area enhanced Al/PDMS triboelectric nanogenerator using novel overlapped microneedle arrays and its application to lighting and self-powered devices. *Applied Surface Science*, 508, 145310.
- Dargusch, M., Liu, W. D. & Chen, Z. G. 2020. Thermoelectric generators: alternative power supply for wearable electrocardiographic systems. *Advanced Science*, 7, 2001362.
- Dhakar, L., Pitchappa, P., Tay, F. E. H. & Lee, C. 2016. An intelligent skin based self-powered finger motion sensor integrated with triboelectric nanogenerator. *Nano Energy*, 19, 532-540.
- Duffy, M. & Carroll, D. Electromagnetic generators for power harvesting. 2004 IEEE 35th annual power electronics specialists conference (IEEE Cat. No. 04CH37551), 2004. IEEE, 2075-2081.
- Fan, F.-R., Tian, Z.-Q. & Wang, Z. L. 2012. Flexible triboelectric generator. *Nano energy*, 1, 328-334.
- Goh, Q. L., Chee, P.-S. & Lim, E. H. A Parametric Study of a Sponge-Based Triboelectric Energy Harvester. 2020 IEEE-EMBS Conference on Biomedical Engineering and Sciences (IECBES), 2021. IEEE, 158-161.
- Gooding, D. M. & Kaufman, G. K. 2011. Tribocharging and the triboelectric series. *Encyclopedia of Inorganic and Bioinorganic Chemistry*, 1-14.

Hao, D., Qi, L., Tairab, A. M., Ahmed, A., Azam, A., Luo, D., Pan, Y., Zhang, Z. & Yan, J. 2022. Solar energy harvesting technologies for PV self-powered applications: A comprehensive review. *Renewable Energy*.

He, W., Sohn, M., Ma, R. & Kang, D. J. 2020. Flexible single-electrode triboelectric nanogenerators with MXene/PDMS composite film for biomechanical motion sensors. *Nano Energy*, 78, 105383.

I-STEM. *COMSOL Multiphysics* [Online]. I-STEM. Available: <https://www.istem.gov.in/istem-comsol> [Accessed].

Jia, Y., Jiang, Q., Sun, H., Liu, P., Hu, D., Pei, Y., Liu, W., Crispin, X., Fabiano, S. & Ma, Y. 2021. Wearable thermoelectric materials and devices for self-powered electronic systems. *Advanced Materials*, 33, 2102990.

Khan, S. A., Rahimoon, A. Q., Abro, A., Ali, M., Hussain, I. & Ahmed, F. Biomechanical energy harvesting by single electrode-based triboelectric nanogenerator. 2019 2nd International Conference on Computing, Mathematics and Engineering Technologies (iCoMET), 2019. IEEE, 1-5.

Khandelwal, G., Maria Joseph Raj, N. P. & Kim, S. J. 2021. Materials beyond conventional triboelectric series for fabrication and applications of triboelectric nanogenerators. *Advanced Energy Materials*, 11, 2101170.

Lin, Z., Chen, J. & Yang, J. 2016. Recent progress in triboelectric nanogenerators as a renewable and sustainable power source. *Journal of Nanomaterials*, 2016.

Lu, C. X., Han, C. B., Gu, G. Q., Chen, J., Yang, Z. W., Jiang, T., He, C. & Wang, Z. L. 2017. Temperature effect on performance of triboelectric nanogenerator. *Advanced Engineering Materials*, 19, 1700275.

Nguyen, T., Dinh, T., Phan, H.-P., Pham, T. A., Nguyen, N.-T. & Dao, D. V. 2021. Advances in ultrasensitive piezoresistive sensors: from conventional to flexible and stretchable applications. *Materials Horizons*.

Nguyen, V. & Yang, R. 2013. Effect of humidity and pressure on the triboelectric nanogenerator. *Nano Energy*, 2, 604-608.

Padasdao, B. & Boric-Lubecke, O. Respiratory rate detection using a wearable electromagnetic generator. 2011 Annual International Conference of the IEEE Engineering in Medicine and Biology Society, 2011. IEEE, 3217-3220.

Pan, C., Liu, D., Ford, M. J. & Majidi, C. 2020. Ultrastretchable, wearable triboelectric nanogenerator based on sedimented liquid metal elastomer composite. *Advanced Materials Technologies*, 5, 2000754.

Saha, C., O'donnell, T., Wang, N. & McCloskey, P. 2008. Electromagnetic generator for harvesting energy from human motion. *Sensors and Actuators A: Physical*, 147, 248-253.

Shen, J., Li, Z., Yu, J. & Ding, B. 2017. Humidity-resisting triboelectric nanogenerator for high performance biomechanical energy harvesting. *Nano Energy*, 40, 282-288.

Si, J., Duan, R., Zhang, M. & Liu, X. 2022. Recent progress regarding materials and structures of triboelectric nanogenerators for AR and VR. *Nanomaterials*, 12, 1385.

Sojan, S. & Kulkarni, R. K. 2016. A Comprehensive Review of energy harvesting techniques and its potential applications. *International Journal of Computer Applications*, 139, 14-19.

Song, W., Yin, X., Liu, D., Ma, W., Zhang, M., Li, X., Cheng, P., Zhang, C., Wang, J. & Wang, Z. L. 2019. A highly elastic self-charging power system for simultaneously harvesting solar and mechanical energy. *Nano Energy*, 65, 103997.

Sun, L., Chen, S., Guo, Y., Song, J., Zhang, L., Xiao, L., Guan, Q. & You, Z. 2019. Ionogel-based, highly stretchable, transparent, durable triboelectric nanogenerators for energy harvesting and motion sensing over a wide temperature range. *Nano Energy*, 63, 103847.

Tcho, I.-W., Kim, W.-G., Jeon, S.-B., Park, S.-J., Lee, B. J., Bae, H.-K., Kim, D. & Choi, Y.-K. 2017. Surface structural analysis of a friction layer for a triboelectric nanogenerator. *Nano Energy*, 42, 34-42.

Tutorial 13: Modeling Triboelectric Nanogenerators in COMSOL Multiphysics: Part 2, 2021. Directed by Teacheetah.

Unsal, O. & Bedeloglu, A. 2018. Recent trends in flexible nanogenerators: A review. *Mater. Sci. Res. India*, 15, 114-130.

Wan, X., Wang, Z., Zhao, X., Hu, Q., Li, Z., Wang, Z.-L. & Li, L. Flexible and Highly Piezoelectric Nanofibers with Organic-Inorganic Coaxial Structure for Self-Powered Physiological Multimodal Sensing. *Available at SSRN 4156465*.

Wang, H., Han, M., Song, Y. & Zhang, H. 2021a. Design, manufacturing and applications of wearable triboelectric nanogenerators. *Nano Energy*, 81, 105627.

Wang, L., Liu, W., Yan, Z., Wang, F. & Wang, X. 2021b. Stretchable and shape-adaptable triboelectric nanogenerator based on biocompatible liquid electrolyte for biomechanical energy harvesting and wearable human-machine interaction. *Advanced Functional Materials*, 31, 2007221.

Wang, S., Lin, L. & Wang, Z. L. 2015. Triboelectric nanogenerators as self-powered active sensors. *Nano Energy*, 11, 436-462.

- Wang, W., Yu, A., Zhai, J. & Wang, Z. L. 2021c. Recent progress of functional fiber and textile triboelectric nanogenerators: towards electricity power generation and intelligent sensing. *Advanced Fiber Materials*, 1-19.
- Wang, Z. L. & Song, J. 2006. Piezoelectric nanogenerators based on zinc oxide nanowire arrays. *Science*, 312, 242-246.
- Wen, Z. 2020. Design of Electrode Materials for Stretchable Triboelectric Nanogenerators. *Nanogenerators*. IntechOpen.
- Wu, C., Wang, A. C., Ding, W., Guo, H. & Wang, Z. L. 2019. Triboelectric nanogenerator: a foundation of the energy for the new era. *Advanced Energy Materials*, 9, 1802906.
- Xiao, X. 2022. The direct use of enzymatic biofuel cells as functional bioelectronics. *Esience*, 2, 1-9.
- Yang, Y., Zhang, H., Lin, Z.-H., Zhou, Y. S., Jing, Q., Su, Y., Yang, J., Chen, J., Hu, C. & Wang, Z. L. 2013. Human skin based triboelectric nanogenerators for harvesting biomechanical energy and as self-powered active tactile sensor system. *ACS nano*, 7, 9213-9222.
- Zhang, N., Chen, J., Huang, Y., Guo, W., Yang, J., Du, J., Fan, X. & Tao, C. 2016. A wearable all-solid photovoltaic textile. *Advanced Materials*, 28, 263-269.
- Zhang, R. & Olin, H. 2020. Material choices for triboelectric nanogenerators: a critical review. *EcoMat*, 2, e12062.
- Zhao, Z., Dai, Y., Dou, S. & Liang, J. 2021. Flexible nanogenerators for wearable electronic applications based on piezoelectric materials. *Materials Today Energy*, 20, 100690.
- Zhu, J., Hu, Z., Song, C., Yi, N., Yu, Z., Liu, Z., Liu, S., Wang, M., Dexheimer, M. G. & Yang, J. 2021. Stretchable wideband dipole antennas and rectennas for RF energy harvesting. *Materials Today Physics*, 18, 100377.

APPENDICES

Appendix A: Supporting Attachment for Literature Review

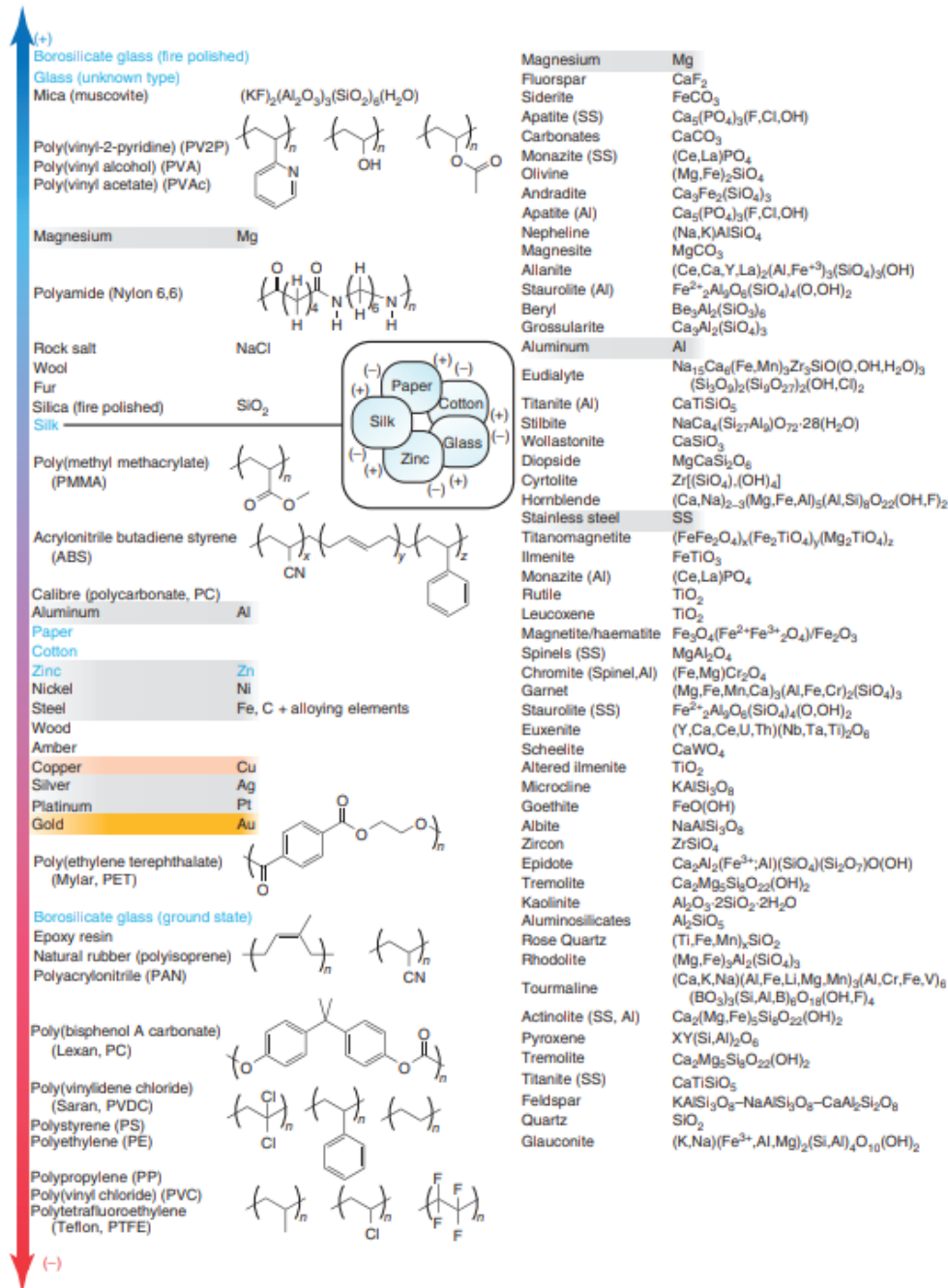


Figure A-1: Triboelectric Series of Polymers, Metals, and Inorganic Compounds (Gooding and Kaufman, 2011).

Appendix B: Supporting Attachments for Ball Bouncing Application

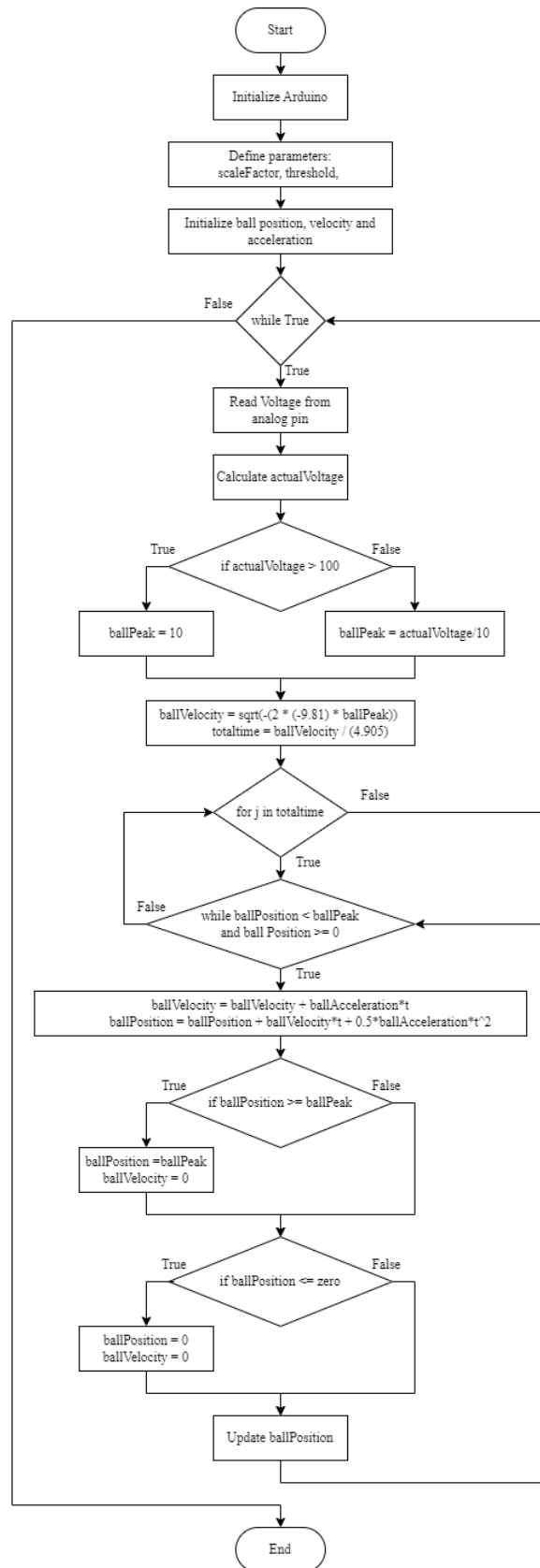


Figure B-1: Flowchart for Ball Bouncing Application.

Code for Ball Bouncing Application:

```

ard = arduino('COM5', 'Uno'); % Initialize Arduino

% Define parameters
R1 = 10000.0; % the resistance of R1 in k?
R2 = 50; % the resistance of R2 in k?
scaleFactor = (R1 + R2) / R2; % the scale factor for the
voltage divider
threshold = 12; % the threshold voltage value

% Define ball parameters
g = 9.81; % gravitational acceleration (m/s^2)
v0 = 0; % initial velocity (m/s) % Change this to get
diff speed
a = -g; % acceleration due to gravity (m/s^2)
dt = 0.02; % time step (s)
bounce = false; % ball bounce

% Initialize voltage vector by t
voltage = zeros(size(t));

% Initialize ball position, velocity and acceleration
ballPosition = 0; % initial position (m)
ballPeak = 0; %The peak position the ball should bounce to (m)
ballVelocity = v0; % initial velocity (m/s)
velocityPeak = 0; % velocity peak (m/s)
ballAcceleration = a; % initial acceleration (m/s^2)
totaltime = 0;

% Initialize Figure for ball bouncing
%figure; % Create a figure window
axis([0 10 0 10]); % Set the axis limits
hold on;
ball = plot(5, 0, 'o', 'MarkerSize', 20, 'MarkerFaceColor',
'b'); % Create a ball object

% Read voltage from analog pin A0 and plot
while true
    % Read voltage from analog pin A0
    reading = readVoltage(ard, 'A1');
    actualVoltage = reading * scaleFactor;

    % Add voltage to vector
    % Turn on LED if voltage is above threshold
    if not(bounce)
        if actualVoltage > threshold
            voltage(i) = actualVoltage;
            bounce = true;

            % Cap ball position at 10 when voltage exceed 100
            if actualVoltage >100
                ballPeak = 10;
            else % Calculate ball position based on voltage
                ballPeak = actualVoltage / 10;
            end

            ballVelocity = sqrt(-(2 * (-9.81) *
ballPeak)) ;%obtain starting velocity required

```

```

        totaltime = ballVelocity / (4.905); % obtain end
time of each bounce

        fprintf('Voltage ='); disp(actualVoltage);
        fprintf('Bouncing peak ='); disp(ballPeak);

    else
        voltage(i) = zero;
        bounce = false;
    end

    ballPosition = 0;
    set(ball, 'YData', ballPosition); % Update the position
of the ball
    drawnow;
    end

    t=0;
    for j = 0.01:dt:totaltime
        t = t+j;
        while ballPosition < ballPeak && ballPosition >= 0 &&
bounce
            ballVelocity = ballVelocity + ballAcceleration*t; %
update velocity
            ballPosition = ballPosition + ballVelocity*t +
0.5*ballAcceleration*t^2; % update position

            if ballPosition >= ballPeak
                ballPosition =ballPeak;
                ballVelocity = 0;
            end

            %Check if ball reach floor
            if ballPosition <= zero
                bounce = false;
                ballPosition = 0;
                ballPeak = 0;
            end

            % Update ball position
            set(ball, 'YData', ballPosition); % Update the
position of the ball
            drawnow;
            pause(0.01);
        end

    end

    clear t;

    ballPosition = 0;
    bounce = false;
    set(ball, 'YData', ballPosition); % Update the position of
the ball
    drawnow;
    % Pause for 0.01 seconds before taking the next reading
    pause(0.01);
end

```


Appendix C: Supporting Attachments for Turn On LED Application

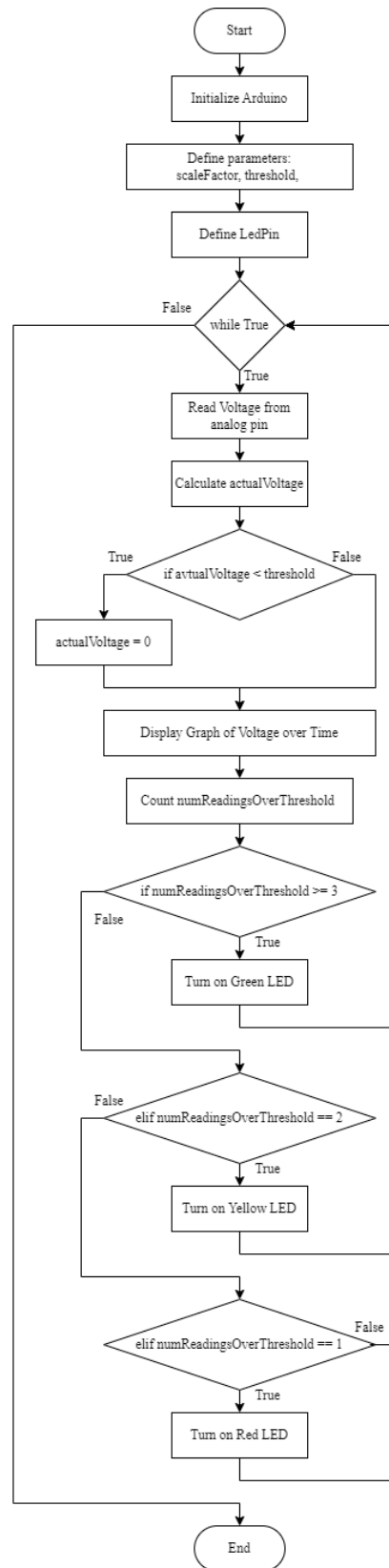


Figure C-1: Flowchart for Turn On LED Application.

Code for Turn On LED Application:

```

ard = arduino('COM5', 'Uno'); % Initialize Arduino

% Define parameters
R1 = 10000.0; % the resistance of R1 in k?
R2 = 50; % the resistance of R2 in k?
scaleFactor = (R1 + R2) / R2; % the scale factor for the
voltage divider
threshold = 12; % the threshold voltage value
readingsSize = 40; % Number of Readings

% Initialize voltage vector by t
voltage = zeros(size(t));
readings = zeros(1, readingsSize); % Initialize readings array
time = linspace(0, readingsSize*0.1, readingsSize); % Time axis
for plot

% Define pin
redLedPin = 'D9';
yellowLedPin = 'D10';
greenLedPin = 'D11';

% Set LED pins as output
configurePin(ard, redLedPin, 'DigitalOutput');
configurePin(ard, yellowLedPin, 'DigitalOutput');
configurePin(ard, greenLedPin, 'DigitalOutput');

% Read voltage from analog pin A0 and plot
while true
    % Read analog input from sensor and convert to voltage
    reading = readVoltage(ard, 'A1');
    voltage = reading * scaleFactor;

    if voltage < threshold
        voltage = 0;
    end

    % Store latest reading in array
    readings = [readings(2:end), voltage];

    % Plot voltage readings over time
    plot(time, readings);
    xlabel('Time (s)');
    ylabel('Voltage (V)');
    title('Voltage Readings over Time');
    drawnow; % Update plot

    % Determine number of readings exceeding the threshold
    numReadingsOverThreshold = sum(readings > threshold);
    fprintf('Number of Readings =');
    disp(numReadingsOverThreshold);

    % Turn on appropriate LED based on number of readings over
    threshold
    if numReadingsOverThreshold >= 3
        writeDigitalPin(ard, greenLedPin, 1);
        writeDigitalPin(ard, yellowLedPin, 0);
        writeDigitalPin(ard, redLedPin, 0);
    end
end

```

```
elseif numReadingsOverThreshold == 2
    writeDigitalPin(ard, greenLedPin, 0);
    writeDigitalPin(ard, yellowLedPin, 1);
    writeDigitalPin(ard, redLedPin, 0);
elseif numReadingsOverThreshold == 1
    writeDigitalPin(ard, greenLedPin, 0);
    writeDigitalPin(ard, yellowLedPin, 0);
    writeDigitalPin(ard, redLedPin, 1);
else
    writeDigitalPin(ard, greenLedPin, 0);
    writeDigitalPin(ard, yellowLedPin, 0);
    writeDigitalPin(ard, redLedPin, 0);
end

% Wait for some time before taking the next reading
pause(0.01);
end
```

Appendix D: Tables of Simulation Results

Table D-1: Potential Difference (V) Generated by Contact Separation Mode of TENG. (Triboelectric Material: PDMS, Electrode: Copper)

Distance (mm)	Bottom Electrode Electric Potential (V)	Top Electrode Electric Potential (V)	Potential Difference (V)
0.0	0.72	-0.75	1.46
1.0	363.82	-376.98	740.80
2.0	623.18	-635.56	1258.73
3.0	828.83	-836.87	1665.70
4.0	999.37	-1002.43	2001.81
5.0	1144.89	-1143.20	2288.09
6.0	1271.46	-1265.72	2537.18
7.0	1383.23	-1373.97	2757.20
8.0	1483.35	-1471.01	2954.36
9.0	1573.84	-1558.85	3132.69
10.0	1656.43	-1639.14	3295.57
11.0	1732.24	-1712.88	3445.12
12.0	1802.22	-1781.22	3583.44
13.0	1867.38	-1844.77	3712.15
14.0	1928.13	-1904.21	3832.33
15.0	1985.22	-1960.03	3945.25
16.0	2038.77	-2012.51	4051.28
17.0	2089.67	-2062.13	4151.81
18.0	2137.62	-2109.14	4246.77
19.0	2183.30	-2153.59	4336.89

Table D-2: Potential Difference (V) Generated by Contact Separation Mode of TENG. (Triboelectric Material: EGaIn Ecoflex, Electrode: Copper)

Distance (mm)	Bottom Electrode Electric Potential (V)	Top Electrode Electric Potential (V)	Potential Difference (V)
0.0	0.71	-0.74	1.46
1.0	362.57	-375.95	738.52
2.0	621.75	-634.15	1255.90
3.0	827.44	-835.21	1662.65
4.0	998.09	-1000.57	1998.66
5.0	1143.71	-1141.18	2284.89
6.0	1270.39	-1263.57	2533.96
7.0	1382.25	-1371.72	2753.97
8.0	1482.45	-1468.67	2951.11
9.0	1573.00	-1556.44	3129.44
10.0	1655.66	-1636.66	3292.32
11.0	1731.52	-1710.35	3441.87
12.0	1801.55	-1778.64	3580.19
13.0	1866.75	-1842.15	3708.89
14.0	1927.53	-1901.55	3829.08
15.0	1984.66	-1957.33	3941.99
16.0	2038.24	-2009.78	4048.03
17.0	2089.16	-2059.38	4148.55
18.0	2137.14	-2106.37	4243.51
19.0	2182.84	-2150.79	4333.63

Table D-3: Potential Difference (V) Generated by Contact Separation Mode of TENG. (Triboelectric Material: PDMS, Electrode: Silver)

Distance (mm)	Bottom Electrode Electric Potential (V)	Top Electrode Electric Potential (V)	Potential Difference (V)
0.0	0.74	-0.76	1.51
1.0	373.18	-382.54	755.73
2.0	636.41	-643.34	1279.74
3.0	844.15	-845.91	1690.06
4.0	1016.01	-1012.34	2028.34
5.0	1162.39	-1153.70	2316.09
6.0	1289.60	-1276.60	2566.20
7.0	1401.85	-1385.19	2787.04
8.0	1502.35	-1482.49	2984.84
9.0	1593.14	-1570.52	3163.66
10.0	1675.98	-1650.95	3326.94
11.0	1752.00	-1724.84	3476.85
12.0	1822.15	-1793.28	3615.42
13.0	1887.46	-1856.93	3744.38
14.0	1948.34	-1916.44	3864.78
15.0	2005.54	-1972.32	3977.86
16.0	2059.20	-2024.88	4084.08
17.0	2110.18	-2074.57	4184.75
18.0	2158.21	-2121.62	4279.83
19.0	2203.95	-2166.12	4370.07

Table D-4: Potential Difference (V) Generated by Contact Separation Mode of TENG with Different Triboelectric Materials and Electrodes.

Distance (mm)	Potential Difference (V)		
	PDMS & Copper	EGaIn & Copper	PDMS & Silver
0.0	1.46	1.46	1.51
1.0	740.80	738.52	755.73
2.0	1258.73	1255.90	1279.74
3.0	1665.70	1662.65	1690.06
4.0	2001.81	1998.66	2028.34
5.0	2288.09	2284.89	2316.09
6.0	2537.18	2533.96	2566.20
7.0	2757.20	2753.97	2787.04
8.0	2954.36	2951.11	2984.84
9.0	3132.69	3129.44	3163.66
10.0	3295.57	3292.32	3326.94
11.0	3445.12	3441.87	3476.85
12.0	3583.44	3580.19	3615.42
13.0	3712.15	3708.89	3744.38
14.0	3832.33	3829.08	3864.78
15.0	3945.25	3941.99	3977.86
16.0	4051.28	4048.03	4084.08
17.0	4151.81	4148.55	4184.75
18.0	4246.77	4243.51	4279.83
19.0	4336.89	4333.63	4370.07

Table D-5: Potential Difference (V) Generated by Single Electrode Mode of TENG with Different Triboelectric Materials and Electrodes.

Distance (mm)	Potential Difference (V)		
	PDMS & Copper	EGaIn & Copper	PDMS & Silver
0.0	0.063	0.063	0.062
1.0	87.601	87.400	85.861
2.0	137.767	137.489	134.724
3.0	171.582	171.243	167.554
4.0	196.219	195.828	191.426
5.0	215.044	214.612	209.633
6.0	229.912	229.444	223.999
7.0	241.944	241.446	235.618
8.0	251.354	251.354	245.189
9.0	260.186	259.643	253.185
10.0	267.246	266.684	259.988
11.0	273.321	272.744	265.822
12.0	278.574	277.983	270.884
13.0	283.200	282.597	275.331
14.0	287.293	286.679	279.244
15.0	290.918	290.295	282.727
16.0	294.147	293.516	285.823
17.0	297.064	296.425	288.626
18.0	299.703	299.057	291.154
19.0	302.106	301.454	293.459

Table D-6: Potential Difference (V) Generated by Single Electrode Mode of TENG for Distance up to 58 mm.

Distance (mm)	Potential Difference (V)
0.0	0.277
2.0	182.981
4.0	255.828
6.0	295.844
8.0	320.763
10.0	337.577
12.0	349.609
14.0	358.606
16.0	365.574
18.0	371.120
20.0	375.640
22.0	379.389
24.0	382.548
26.0	385.247
28.0	387.576
30.0	389.609
32.0	391.394
34.0	392.978
36.0	394.390
38.0	395.660
40.0	396.804
42.0	397.842
44.0	398.788
46.0	399.652
48.0	400.450
50.0	401.182
52.0	401.860
54.0	402.488
56.0	403.071
58.0	403.615